Accepted Manuscript

Synthesis and biological evaluation of novel benzylidene-succinimide derivatives as noncytotoxic antiangiogenic inhibitors with anticolorectal cancer activity *in vivo*

Kaixiu Luo, Yafeng Bao, Feifei Liu, Chuanfan Xiao, Ke Li, Conghai Zhang, Rong Huang, Jun Lin, Jihong Zhang, Yi Jin

PII: S0223-5234(19)30621-X

DOI: https://doi.org/10.1016/j.ejmech.2019.06.094

Reference: EJMECH 11497

To appear in: *European Journal of Medicinal Chemistry*

Received Date: 19 April 2019

Revised Date: 5 June 2019

Accepted Date: 30 June 2019

Please cite this article as: K. Luo, Y. Bao, F. Liu, C. Xiao, K. Li, C. Zhang, R. Huang, J. Lin, J. Zhang, Y. Jin, Synthesis and biological evaluation of novel benzylidene-succinimide derivatives as noncytotoxic antiangiogenic inhibitors with anticolorectal cancer activity *in vivo*, *European Journal of Medicinal Chemistry* (2019), doi: https://doi.org/10.1016/j.ejmech.2019.06.094.

Abstract

Synthesis and biological evaluation of novel benzylidene-succinimide derivatives as non-cytotoxic anti-angiogenic inhibitors with anti-colorectal cancer activity *in vivo*

Kaixiu Luo,[‡a] Yafeng Bao,[‡b] Feifei Liu, [‡b] Chuanfan Xiao,[‡a] , Ke Li,[c] Conghai Zhang,[a] Rong Huang,[a] Jun Lin,*[a] Jihong Zhang*[b] and Yi Jin*[a]

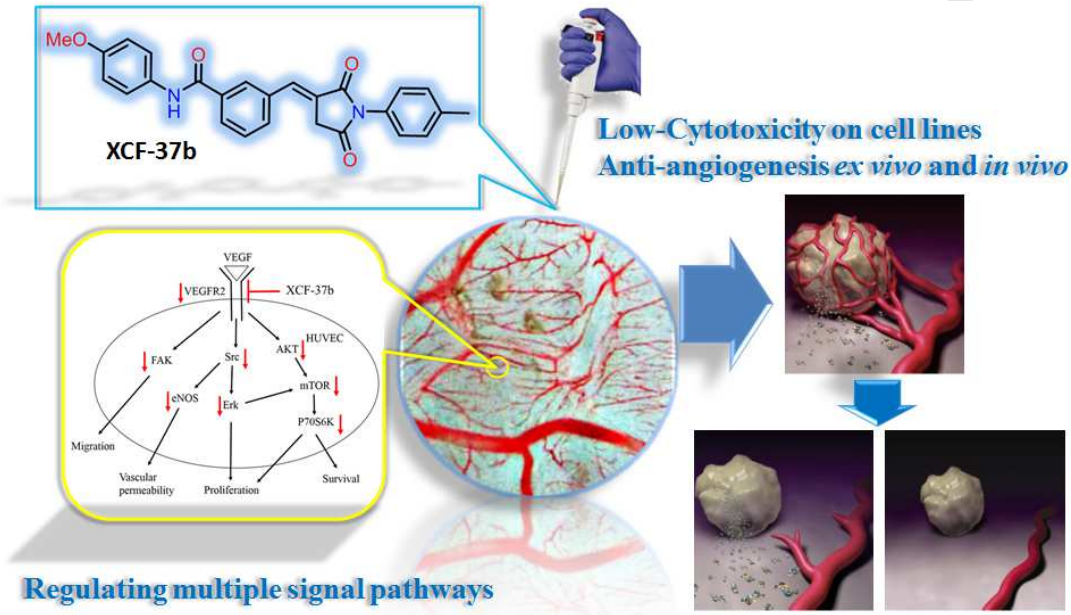

Synthesis and biological evaluation of novel benzylidene-succinimide derivatives as noncytotoxic antiangiogenic inhibitors with anticolorectal cancer activity *in vivo*

Kaixiu Luo,[‡a] Yafeng Bao,[‡b] Feifei Liu, [‡b] Chuanfan Xiao,[‡a] , Ke Li,[c] Conghai Zhang,[a] Rong Huang,[a] Jun Lin,*[a] Jihong Zhang*[b] and Yi Jin*[a]

a. Key Laboratory of Medicinal Chemistry for Natural Resource, Ministry Education and Yunnan Province, School of Chemical Science and Technology, Yunnan University, Kunming, 650091, P. R. China.

b. Laboratory of Molecular Genetics of Aging and Tumor, Medical School, Kunming University of Science and Technology, Kunming, 650500, P. R. China.

c. Biomedical Department, Yunnan Cancer Hospital, the Third Affiliated Hospital of Kunming Medical University, Kunming, 650118, P. R. China.

‡ the authors contributed equally to this work.

***** Corresponding author. Tel./fax: +86-871-6503-3119. E-mail: linjun@ynu.edu.cn (J. Lin); zhjihong2000@126.com (JH. Zhang); jinyi@ynu.edu.cn (Y. Jin).

Keywords: arylmethylene succinimide; angiogenesis; colon cancer; noncytotoxic; mTOR; matrix metalloproteinase; hypoxia-inducible factor-1α.

Abstract

A novel series of benzylidene-succinimide derivatives were synthesized, characterized and evaluated for their cytotoxicities against HCT116, and SW480 cancer cells and NCM460 normal human cells. Their antiangiogenic capabilities were evaluated using a chick chorioallantoic membrane (CAM) assay. The compound, **XCF-37b**, was selected as the most potent antiangiogenic inhibitor with noncytotoxicity to evaluate the pharmacological effects on human umbilical vein endothelial cells (HUVECs) and cancer cells *in vivo* and *in vitro*. The results showed that **XCF-37b** inhibited HT29-cell colon tumor growth *in vivo*, without showing cytotoxicity against the five other cancer cell lines *in vitro*. Experiments confirmed that **XCF-37b** had obvious antiangiogenic activity by HUVEC migration and invasion and rat aortic ring angiogenesis *ex vivo*. Mechanism studies showed that **XCF-37b** inhibited the AKT/mTOR and VEGFR2 signaling pathways, as evidenced by decreased expressions of phosphor-AKT (p-AKT), p-mTOR, p-VEGFR2 (Tyr175), p-Src (Tyr416), p-FAK (Tyr925), and p-Erk1/2 (Thr202/Tyr204). Moreover, **XCF-37b** significantly decreased the protein expressions of matrix metalloproteinase-2 (MMP-2), MMP-9 and hypoxia-inducible factor-1α (HIF-1α). **XCF-37b** generally regulated angiogenic inhibition through several regulatory pathways, without significantly interfering with colorectal cancer cell growth.

1. Introduction

Colorectal cancer (CRC) is ranked as one of the three most common cancers and one of the three leading causes of cancer-related deaths worldwide.[1-3] Despite the developments in clinical oncology in recent decades, CRC recurrence and chemotherapy resistance remain critical problems in effectively treating patients with CRC.[4, 5] Because approximately 50% of patients do not respond to CRC treatment, new therapeutic medications are urgently needed to improve the curative efficacy and decrease the toxicity of ineffective treatments in patients with CRC.[6]

Several mechanisms have been proposed as chemotherapeutic strategies for treating patients with CRC, including cytotoxic chemotherapy and targeted therapies across multiple lines of treatment,[7] clearance of cancer stem cells,[8] epigenetic modification,[9] and CRC antiangiogenesis.[10, 11] Tumor angiogenesis plays a crucial role in regulating invasion and metastasis.[12, 13] Dozens of proangiogenic factors have been identified as potential targets for developing angiogenic inhibitors. Reducing the expressions of angiogenesis-related proteins, such as the vascular endothelial growth factor (VEGF) family proteins, has been demonstrated to significantly suppress endothelial survival, mitogenesis, differentiation, migration, and vascular permeability[14-16] and to decrease the expressions of the metastasis-associated proteins, matrix metalloproteinase-2 (MMP-2) and MMP-9.[17] In addition, VEGF receptor and several signaling cascades, such as Ras-MAPK, Scr-FAK, and AKT-mTOR, dominate in tumor initiation and progression and regulate essential cellular functions, including survival, proliferation and angiogenesis.[18, 19] These pathways are also abnormal in many cancers, including CRC.[20, 21] For example, blocking AKT-mTOR overactivity has antitumor effects on colon cancer cells.[22] Moreover, hypoxia-inducible factor-1α (HIF-1α) is a transcriptional factor controlling genes involved in glycolysis, angiogenesis, invasion, and metastasis of tumor progression.[23] Under hypoxic conditions, the stabilized HIF-1α/HIF-1β dimer translocates into the nucleus to activate the transcription of target genes including VEGF;[24] thus, regulating the nuclear translocation of HIF-1α effectively inhibits tumor angiogenesis. However, current antiangiogenic clinical medications, such as ramucirumab, sorafenib, and regorafenib, still have limitations in antiangiogenic therapies including cytotoxicity, drug resistance, reduced drug delivery, increased hypoxia, and tumor metastasis. Treating malignant tumors effectively with low toxicity remains a major challenge and is urgently needed. The original concept of

antiangiogenesis therapy involved "tumor starvation" via reduced vascularization as the primary mechanism.[12] Therefore, to inhibit tumor angiogenesis without producing cytotoxicity, novel angiogenic inhibitors must be developed.[25-28] Herein, we designed and synthesized a novel series of benzylidene-succinimide derivatives, which showed obvious antiangiogenic activity upon biological evaluation. These compounds had no obvious cytotoxicity on several cancer cell lines and normal human colon epithelial cells.

2. Results and discussion

2.1. Compound design strategy

Michael conjugate addition is an effective method of elaborating interactions between drugs and receptor proteins.[29-31] Maleimides are excellent Michael acceptors, which usually form succinimide derivatives. Substances bearing a succinimide fragment have been found in many natural products and in some candidate drugs (**Fig. 1**), such as moiramide B and andrimide, which are highly specific antibiotics,[32] longimide A/B, which has antitumor activity,[33] and GNX-686, which has antiangiogenic properties.[34]

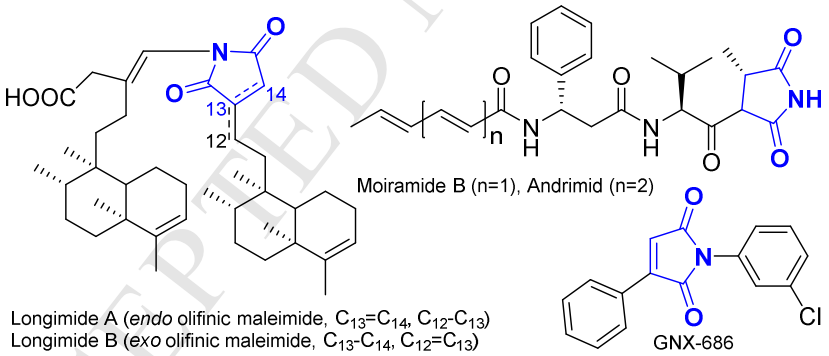

Fig. 1. Representative bioactive compounds bearing a succinimide fragment

Michael addition of thiols or amines to endocyclic C=C bonds of maleimides is the site-specific drug-protein bioconjugation under physiological conditions for several marketed drugs (**Fig. 2a,** route i).[35] However, this methodology has a major drawback in that the resulting thio-succinimidyl adducts 3 are prone to involving an exchange reaction with more active nucleophilic substrates (e.g., cysteine residues of the proteins *in vivo*; **Fig. 2a,** route ii).[36-39] To overcome the instabilities of the adducts 3, a method was developed to form relatively stable ring-opened thiol adducts via hydrolysis under a positive environment (**Fig. 2a,** route iii).[36, 37] However, this approach is not an ideal application because it introduces an additional negative

charge in the ring-opened products (6 and 7), which may make it difficult for cellular internalization of cell-penetrating medications. Consequently, developing stable Michael-adduct-forming maleimide derivatives is highly attractive to pharmaceutical chemists. Recently, Kalia et al. reported that exocyclic olefinic maleimides can form highly stable thio-Michael adducts that resist thiol exchange under physiological conditions (**Fig. 2b**).[40] Although some active molecules bearing a benzylidene-succinimide unit show potent GPR119 agonistic activity,[41] inhibit DDX and HIV-1 replication,[42] and have oral activity for treating induced acute liver injury,[43] to our knowledge, benzylidene-succinimide derivatives remain unreported in tumor antiangiogenesis applications. Thus, after previously exploring potential angiogenic inhibitors,[44-46] we aimed to design benzylidene-succinimide derivatives with potent antiangiogenic activity and antitumor properties *in vivo*. As many of the marketed antiangiogenic medications have a terminal amide modification (e.g., sorafenib,[47] regorafenib,[48] and sunitinib[49]), we reasoned that a benzylidene-succinimide fragment bearing a terminal amide unit (**Fig. 2c**) would possess this pharmacological attribute.

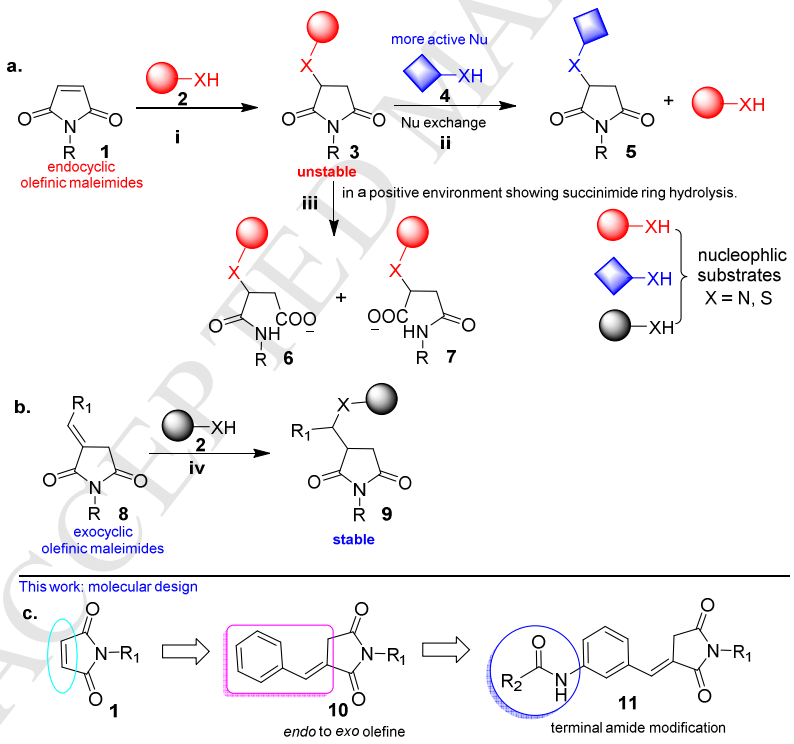

Fig 2. a) Conventional methodology for bioconjugation between a maleimide and a protein using endocyclic olefinic maleimide. b) Kalia's approach using exocyclic olefinic maleimides. c) Molecular design for the current work.

2.2. Chemistry

Scheme 1 illustrates the general synthetic approach for benzylidene-succinimide derivatives (h). First, 4-(arylamino)but-2-enoic acid (c) was prepared using maleic anhydride and amine in acetone or ethyl acetate solvent with a yield of over 97%. To prevent self-polymerization of the intermediate (**c**), the reaction rate and temperature were controlled by slowly adding substituted aniline in an ice bath. The intermediate (c) then underwent the condensation ring-closure reaction catalyzed by triethylamine in an acetic anhydride solvent to form N-substituted maleimide. To obtain the optimum yield in this step, we investigated the reaction conditions at different dosage ratios of 4-(phenylamino)but-2-enoic acid (c1), acetic anhydride and triethylamine at different temperatures. The results showed that the optimum yield (over 90%) could be obtained at a mixing (molar) ratio of 1:6:0.5 at 50°C for the three substrates. Referring to Kalia's method,[40] the catalytic condition of 4-nitrophenole and 1,4-addition of PPh_3 to N-substituted maleimide (d) followed by the Wittig reaction with 3-carboxybenzaldehyde (e) can obtain the 3-carboxybenzylidene-N-substituted-succinimide (f) at room temperature with good yields of 75–95%. The double bond in the products was assigned to *E* configuration by NOE analysis (**Fig. 1S,** SI).[50, 51] In this step, we screened the reaction effect in different solvents and found that the reaction yields in non-proton solvents (e.g., DCM, THF or toluene) were not ideal, but in proton solvents (e.g., EtOH or MeOH), the yields could reach over 90%. Finally, the target products (g) were prepared by a condensation reaction of intermediate (f) and alkyl/arylamine. Because the intermediate is poorly soluble (f), the effects of different solvent combinations (e.g., DMF+DCM or DMF+MeOH) and condensation agents (e.g., HOBT+EDCI or HOBT+TBTU) were investigated. The experimental results showed that the benzylidene-succinimide derivatives (**g**) can be obtained in medium-to-high yield (50–90%) at room temperature using a mixed solvent (DMF:DCM=1:5) and HOBT+TBTU (molar ratio = 1:1) as the condensation reagent.

Scheme 1. General preparation methods for 2-aryl benzoxazoles derivatives.

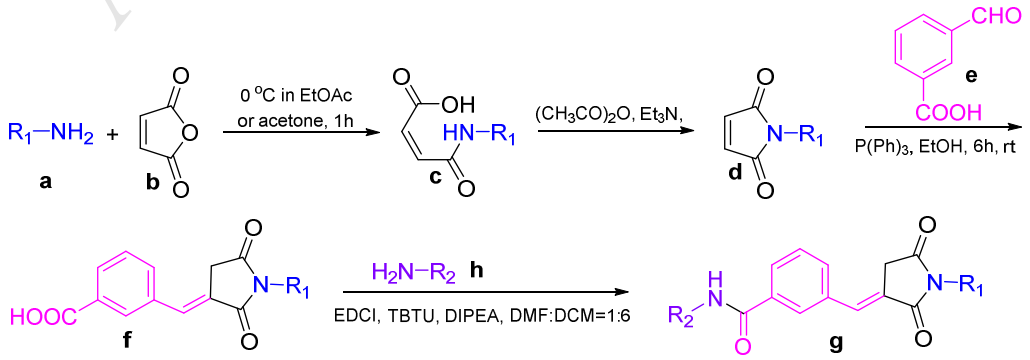

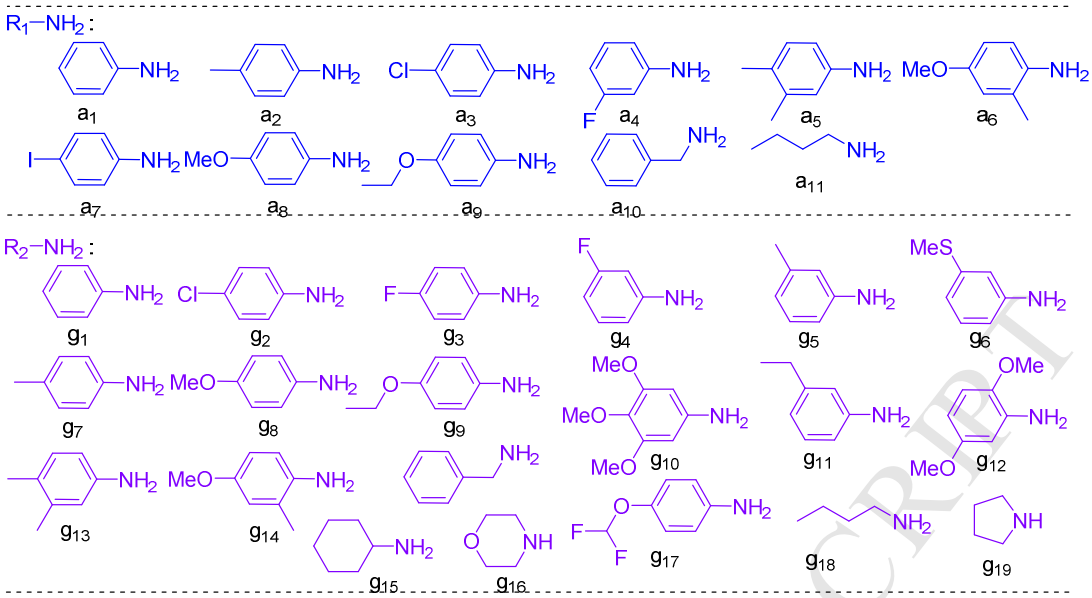

2.3 In vitro cytotoxicity assay

We first synthesized twenty 3-amidobenzylidene-N-phenyl-succinimide compounds (**Table 1**, **g1**–**g20**) with different amide substituents, which were evaluated for cell growth cytotoxicities against two colon cancer cell lines (HCT116 and SW480) using the standard MTT assay, with cisplatin as the reference control. Neither the alkyl amides (**g5**–**g8**) nor most aryl amides exhibited obvious cytotoxicities against the growth of both cancer cell types. However, when the substituents of arylamino were 4-ethoxy aniline, 3-(methylthio)aniline, or 3-ethylaniline, respectively, compounds **g13** (IC_{50}= 84.83μM and 91.45 μM), **g15** (IC_{50}= 65.23 μM and 74.29 μM) and **g20** (IC_{50}= 81.21μM and 88.64 μM) showed inhibition in both HCT116 and SW480 cells.

To investigate the effect of different N-substituted succinimides on inhibitory activities, three N-substituted succinimide compounds (N-p-tolyl **g21**–**g24**, N-butyl **g25**–**g29**, and N-benzyl **g30**–**g33**) were prepared (**Table 2**, **g21**–**g33**). The *in vitro* assay results showed that most of the compounds with these three N-substituents had no significant cytotoxicities. Notably, the compounds bearing 4-ethoxy aniline or a 3-ethylaniline group in the arylamino moiety (**g23**, **g25**, **g31**, and **g32**) exhibited cytotoxicities. We also prepared the hydrogenated product (**g34**) of compound **g24**, which showed no cytotoxicity against these cell lines.

Finally, we evaluated the cytotoxicities of the synthesized compounds on the NCM460 cell line (normal human colon epithelial cells). No compounds showed cytotoxicities against this cell line, confirming the feasibility of designing the benzylidene-succinimide derivatives as noncytotoxic antiangiogenic inhibitors.

Table 1. Cytotoxic effects *in vitro* of synthesized compounds **g1-g20**.

Cpd	Structure	*in vitro* anti-proliferative effects (IC_{50}, μM)[a]		
		HCT116	SW480	NCM460
Control	Cisplatin (DDP)	5.59±0.23	10.02±0.37	17.10±0.30
g1	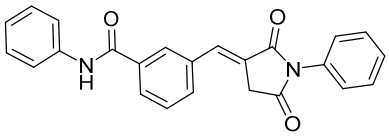	>100	>100	>100
g2	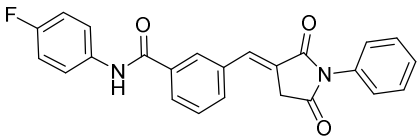	>100	>100	>100
g3	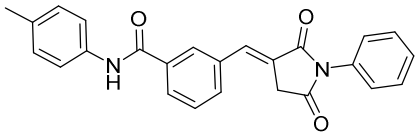	>100	>100	>100
g4	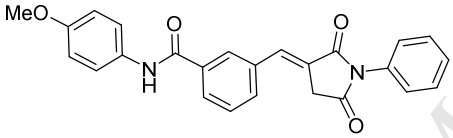	>100	>100	>100
g5	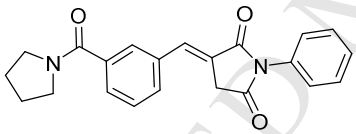	>100	>100	>100
g6	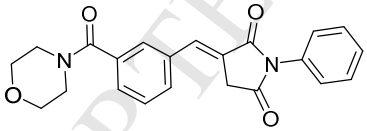	>100	>100	>100
g7	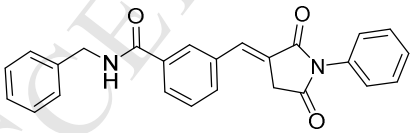	>100	>100	>100
g8	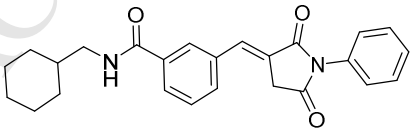	>100	>100	>100
g9	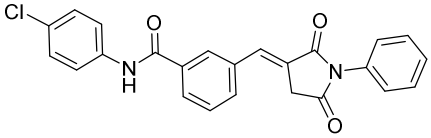	>100	>100	>100

g10	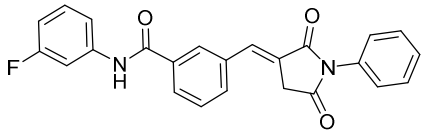	>100	>100	>100
g11	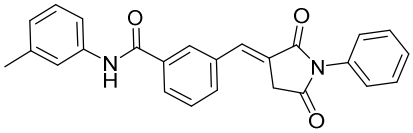	>100	>100	>100
g12	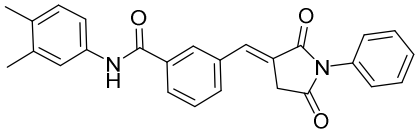	>100	>100	>100
g13	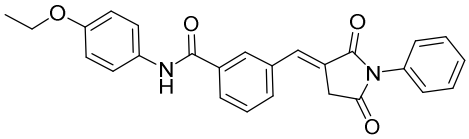	84.83±3.65	91.45±2.18	>100
g14	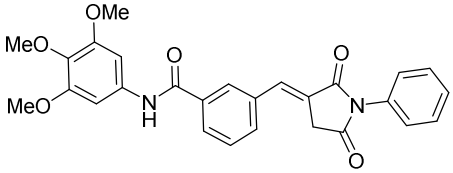	>100	>100	>100
g15	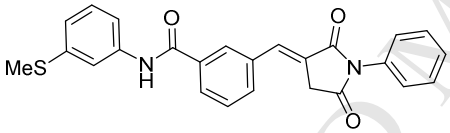	65.23±1.85	74.29±0.87	>100
g16	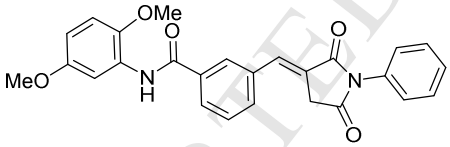	>100	>100	>100
g17	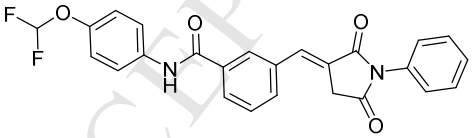	>100	>100	>100
g18	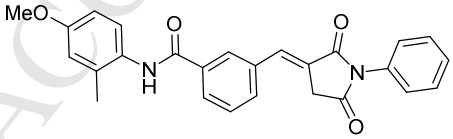	>100	>100	>100
g19	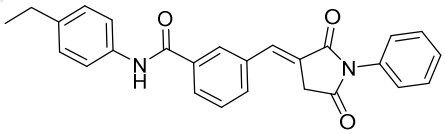	>100	>100	>100
g20	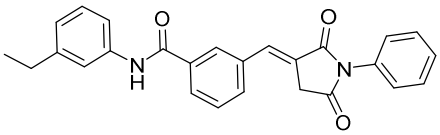	81.21±2.75	88.64±1.82	>100

[a] IC_{50} values are presented as the mean values of at least three independent experiments.

Table 2. Cytotoxic effects *in vitro* of synthesized compounds **g21-g33**.

Cpd	Structure	*in vitro* anti-proliferative effects (IC_{50}, μM)[a]		
		HCT116	SW480	NCM460
Contral	Cisplatin (DDP)	5.31±0.28	9.54±0.17	14.37±0.42
g21	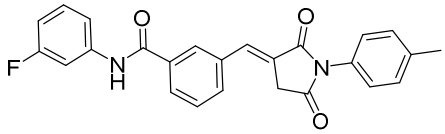	>100	96.85±3.57	>100
g22	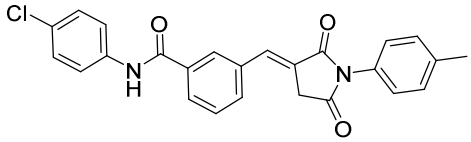	>100	>100	>100
g23	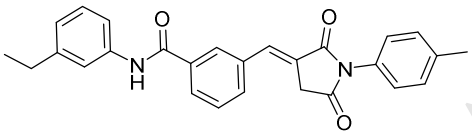	41.53±2.73	65.34±3.68	>100
g24 **(XCF-37b)**	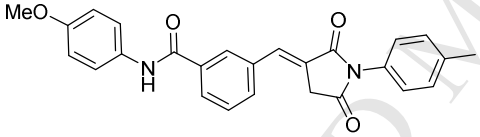	>100	92.98±4.62	>100
g25	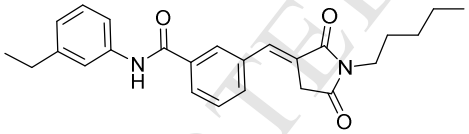	75.32±3.94	83.25±2.73	>100
g26	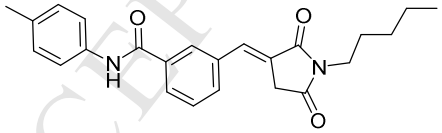	>100	>100	>100
g27	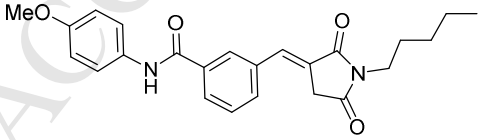	>100	>100	>100
g28	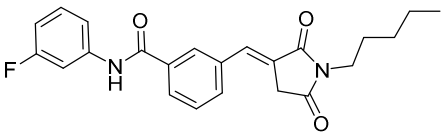	>100	>100	>100
g29	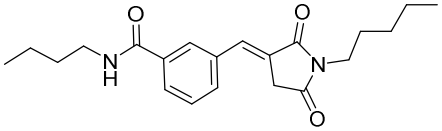	>100	>100	>100

g30	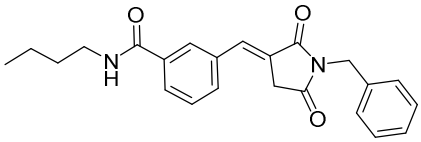	95.05±4.27	>100	>100
g31	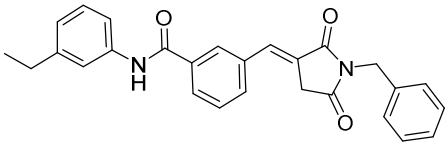	80.60±2.69	91.48±4.18	>100
g32	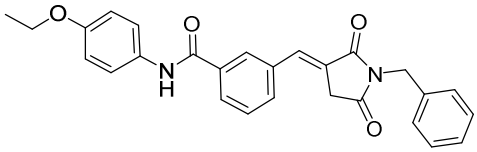	41.70±1.74	73.21±3.27	>100
g33	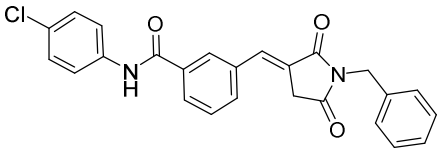	>100	>100	>100
g34[b]	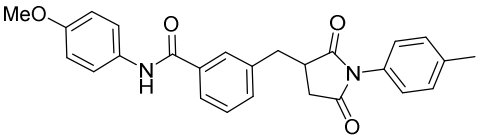	>100	>100	>100

[a] IC_{50} values are presented as the mean values of at least three independent experiments.

[b] The compound was prepared by double-bond hydrogenation of **XCF-37b** (see experimental section).

2.4 Antiangiogenesis screening via chick chorioallantoic membrane (CAM) assay

The CAM assay, an inexpensive, reliable, simple, and convenient biological method, was selected to initially evaluate the synthesized compounds for their angiogenic inhibitory effects. First, compounds **g1**–**g20** were screened to study the extent of new blood vessel formation, which represents the antiangiogenic strength. **Fig. 3a** shows the inhibitory effects compared with normal saline (the blank control) and sunitinib (the positive control). The antiangiogenic activities of the compounds were semiquantitatively analyzed using GraphPad Prism 5.0 (**Fig. 3b**). The results showed that the five compounds **g4**–**g9** exhibited some antiangiogenic activities, but none were as active as the positive control. Subsequently, the compounds **g21**–g34 were screened using the CAM assay (**Fig. 4a)**. The results showed that **g24** (**XCF-37b**) and **g29** exhibited the same antiangiogenic activities as sunitinib. Exposure to **XCF-37b** drastically impaired neovascularization with the absence of vascular networks (**Fig. 4b**). Quantitative analysis revealed that 20 nmol **XCF-37b** reduced the number of blood vessels by 96.4% compared with the saline control. These results confirmed the antiangiogenic potential of **XCF-37b** through an *ex vivo* assay. An *in vivo* mouse

Matrigel plug model of angiogenesis was compared with the control. VEGF-supplemented Matrigels appeared red, indicating the formation of a functional vasculature inside them; however, with **XCF-37b** treatment, the red color in the Matrigels diminished (**Fig. 4c**). Intriguingly, the hydrogenated product **g34** of **XCF-37b** showed moderate antiangiogenic activity. This result implied that the double bond of benzylidene-succinimide contributed to antiangiogenic effect.

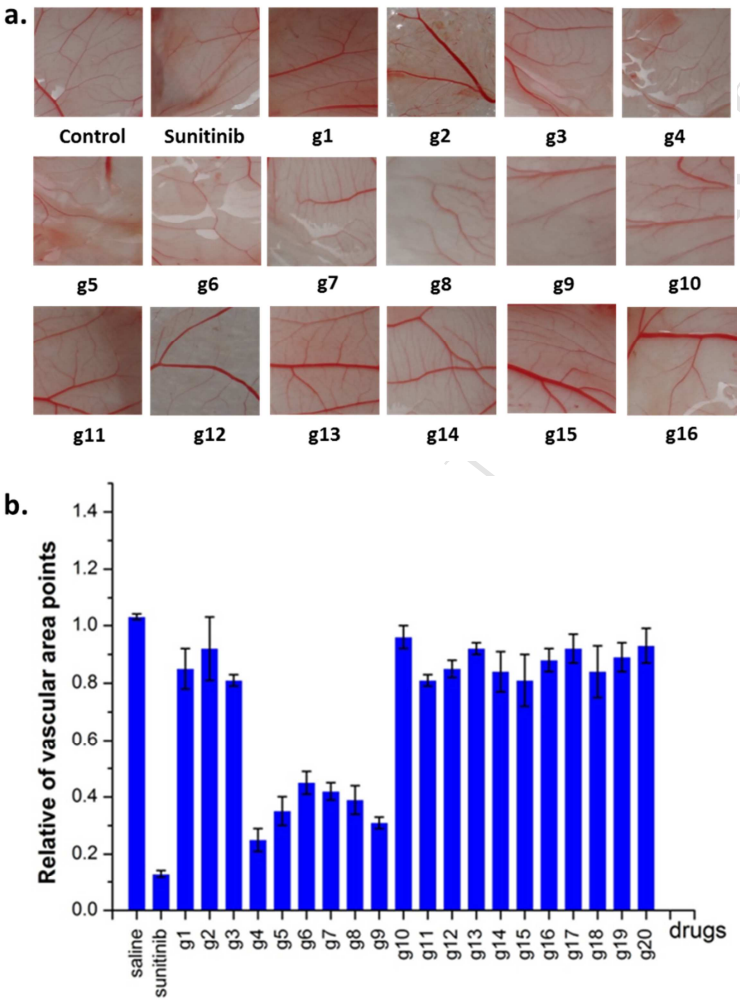

Fig. 3. a) Effect of compounds **g1**–**g16** on CAM blood vessel growth (10 nM/eggs). b) Quantification of the effect of compounds **g1**–**g20** on tube formation shown in the bar graph. The bars show the mean ± SD (n=3) values.

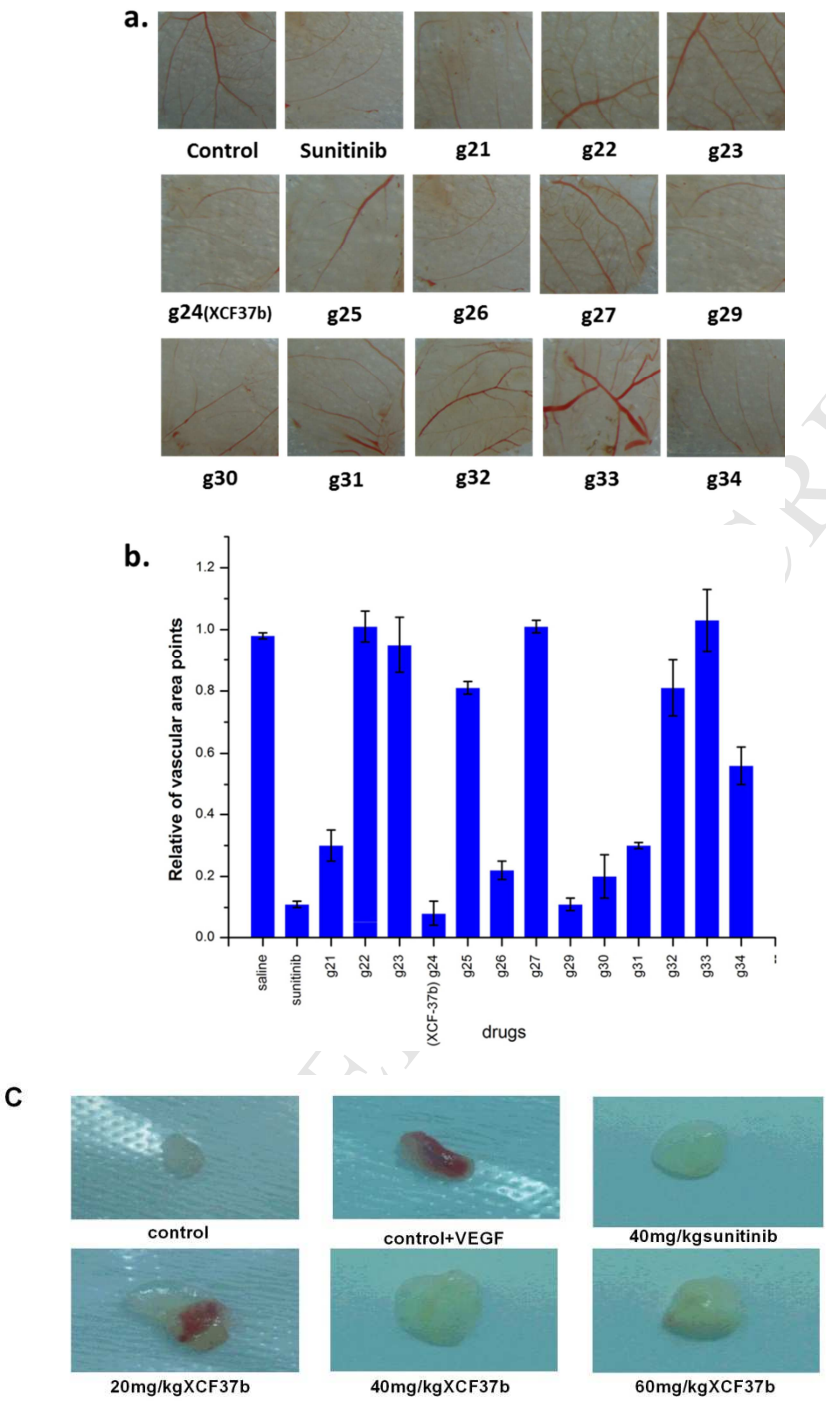

Fig. 4. a) Effect of compounds **g21**−**g34** on CAM blood vessel growth (10 nM/eggs). b) Quantification of the effect of compounds **g21**–**g34** on tube formation shown in the bar graph. The bars show the mean ± SD (n=3). c) *In vivo* angiogenesis assay, Matrigel alone or with VEGF indicated concentrations of compounds were injected into the flanks of Balb/c nude mice, and 15 days later, the mice were sacrificed, and the Matrigel plugs were removed, weighed and photographed.

2.5 XCF-37b *inhibited HUVEC and other cancer cell proliferation*

Suppression of HUVEC growth and proliferation is another critical aspect of angiogenesis. To assess the antiangiogenic activity of **XCF-37b** *in vitro*, the inhibitory effects on VEGF-induced endothelial cell proliferation were evaluated using an MTT assay. VEGF plays an important role in neoangiogenesis in endothelial cells.[52] **XCF-37b** inhibited HUVEC cell proliferation concentration-dependently. Moreover, **XCF-37b** significantly inhibited VEGF-induced proliferation of HUVECs with an IC_{50} value of 8.56 μM compared with those without VEGF stimulation (IC_{50} = 26.58 μM; **Table 3**).

To determine whether **XCF-37b** possesses any cytotoxicity against other human cancer cell lines, a growth inhibition assay was performed, and the results showed IC_{50} values >100 μM in HCT116, SW480, HT29, PC-3 and HepG2 cells (**Table 3**).

Table 3. *In vitro* antiproliferative effects of compound **XCF-37b**. [a]

Compound	HUVEC	HUVEC+VEGF	HCT116	SW480	HT29	PC-3	HepG2
Sunitinib	6.46±0.23	3.63±0.24	NT	NT	NT	NT	NT
DDP	NT	NT	7.062±1.786	9.338±1.544	7.23±0.155	6.04±0.586	2.79±0.226
XCF-37b	26.58±2.17	8.56±2.0	>100	92.985±0.325	>100	>100	>100

[a] IC_{50} values are presented as the mean values from at least three independent experiments.

2.6 XCF-37b *suppressed HUVEC migration and invasion*

Endothelial cell migration and invasion are key events in angiogenesis. To investigate the effect of **XCF-37b** in endothelial cell migration, a wound healing migration assay was performed. HUVEC cells were wounded with tips, followed by a 12-h starvation, then treated with **XCF-37b** (1 μM and 2.5 μM) for 6, 12, and 24 h. The control cells nearly completely migrated to fill the initial clear area after 24 h, while **XCF-37b** treatment significantly reduced VEGF-induced HUVEC cell migration both dose- and time-dependently **(Figure 5b)**. **XCF-37b** (2.5 μM) suppressed HUVEC migration by 30%, 50% and 60% at 6, 12, and 24 h, respectively, compared with the control. Similarly, **XCF-37b** also induced dose-dependent suppression of the VEGF-induced invasion of HUVEC cells (**Figure 5a**). **XCF-37b** treatment at 1 μM, 5 μM, 10 μM and 20 μM suppressed HUVEC cell invasion by 20%, 40%, 50% and 70%, respectively. This study demonstrated that **XCF-37b** suppressed angiogenesis by inhibiting endothelial cell migration and invasion.

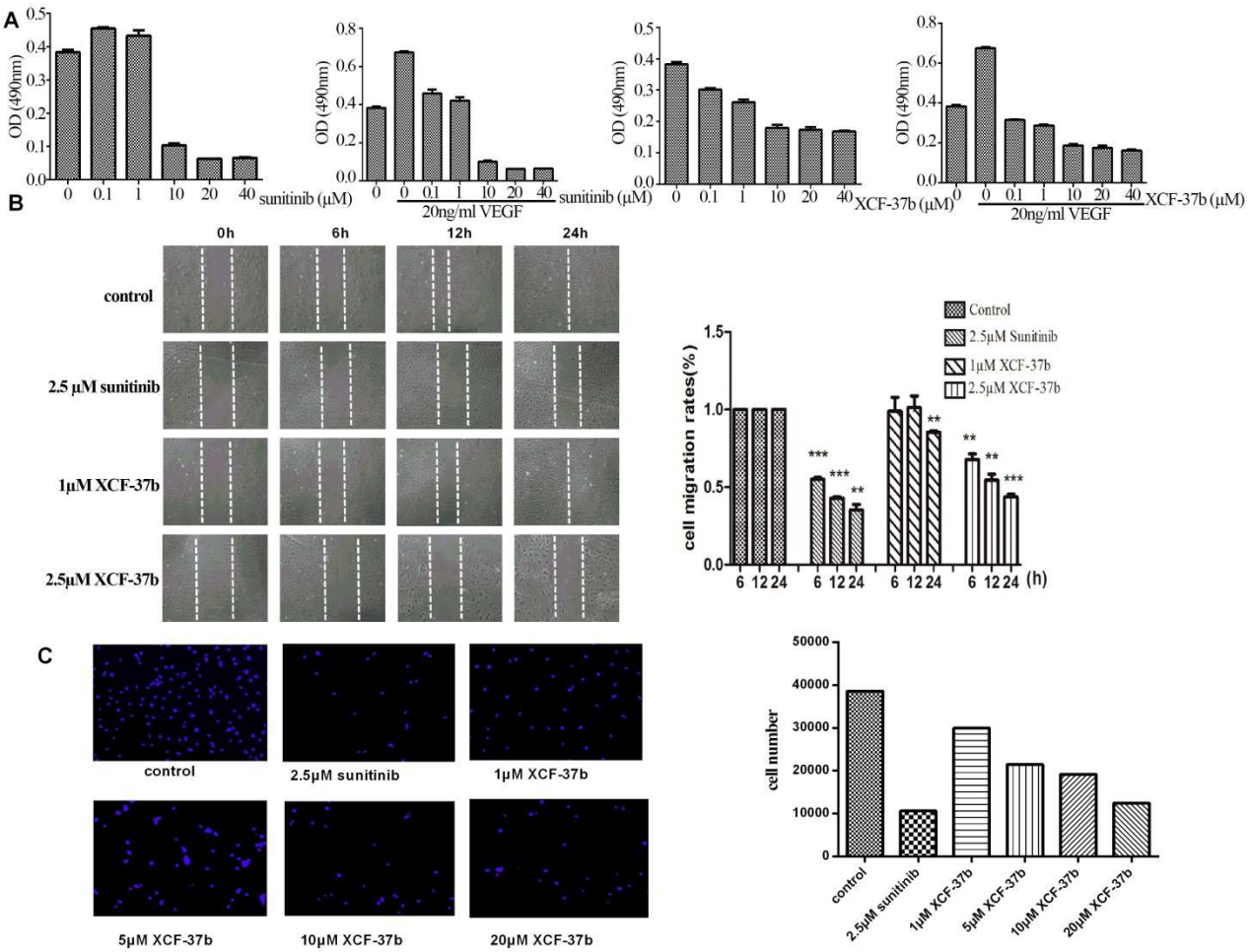

Fig. 5 XCF-37b inhibited HUVEC proliferation, migration, and invasion.

At the later stage of angiogenesis, endothelial cells rearrange themselves into tubes to form capillaries. To further determine the antiangiogenic effects of **XCF-37b** on VEGF-induced endothelial cell capillary-like structure formation, a two-dimensional Matrigel tube formation assay was applied. HUVECs seeded on the Matrigel surface became elongated and formed capillary-like structures, and VEGF significantly enhanced the capillary-like network. However, **XCF-37b** concentration-dependently abrogated the capillary-like network formation. We observed that 1 μM, 2.5 μM and 5 μM of **XCF-37b** treatment inhibited HUVEC capillary tube formation by 30%, 73%, and 80%, respectively, after 6 h compared with the VEGF control. We investigated the effects of **XCF-37b** on microvessel sprouting from vascular tissues using an *ex vivo* rat aortic ring assay. Microvessels emerging from cultured rat aorta embedded in the Matrigel mimicked several stages of angiogenesis, including endothelial proliferation, migration and tube formation. As **Fig. 6a shows**, VEGF significantly initiated microvessel sprouting and formed a complex microvessel

network around the aortic rings. However, treatment with **XCF-37b** at 1 μM, 5 μM, 10 μM, or 20 μM dramatically dose-dependently suppressed capillary sprouting, with 95% inhibition observed at 20 μM, suggesting that **XCF-37b** suppresses VEGF-induced angiogenesis *ex vivo*. In addition, **XCF-37b** at 1–5 μM alone had no obvious cytotoxicity on HUVECs after incubation with cells for 48 h. The results implied that the inhibition of VEGF-induced formation in the cells was not due to cytotoxicity (**Fig. 6b**).

Formation of the VEGF-induced elongated and robust tube-like structures in the HUVEC cells was concentration-dependently abrogated by **XCF-37b**.

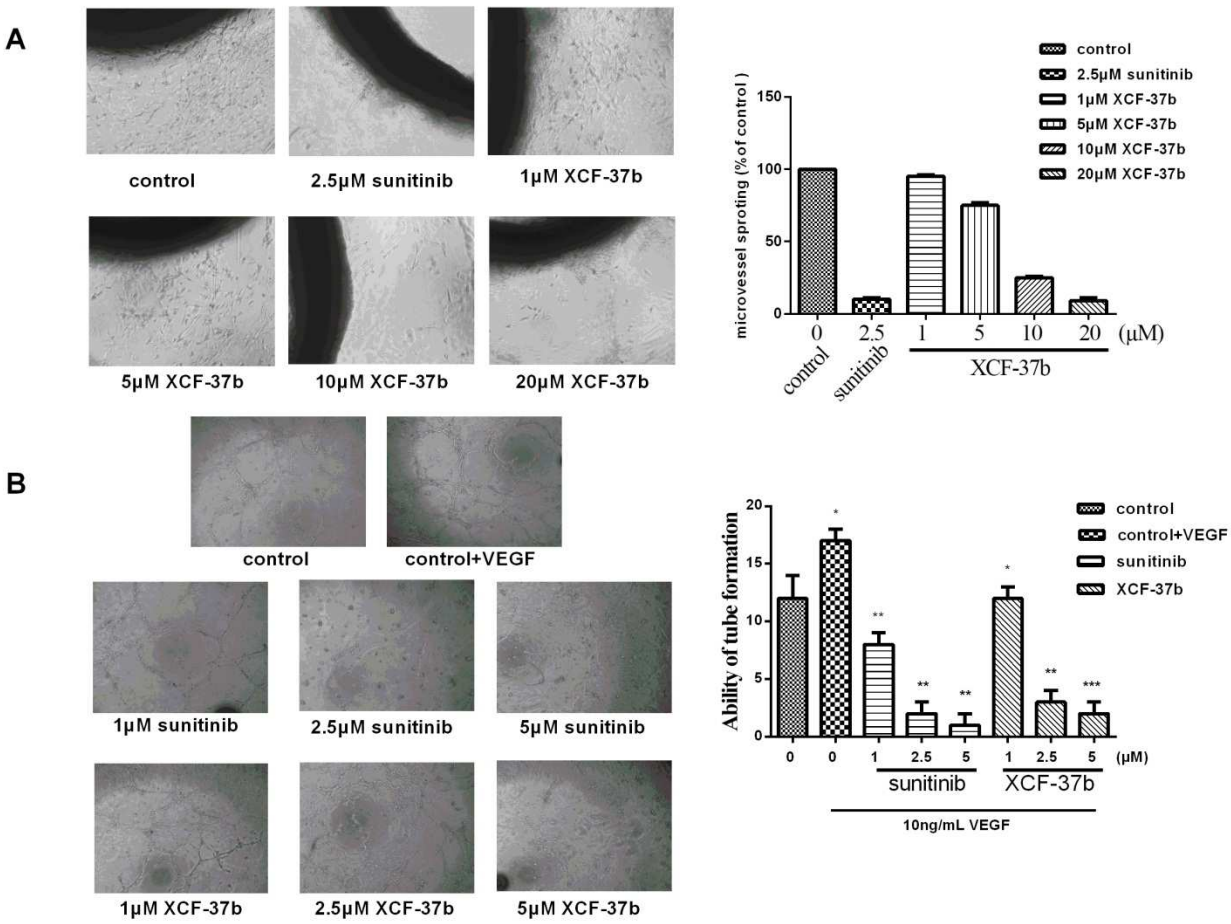

Fig. 6 XCF-37b inhibited *ex vivo* and *in vivo* angiogenesis. a) In the rat aortic ring assay, rat aortic ring sections were embedded in Matrigel and cultured in the opti-MEM medium. After 1 day of starvation, treatments were started and continued with the indicated compound concentrations every 3 days for 7 days. On day 7, images were taken using inverse microscopy. b) Using a tube-formation assay, HUVECs suspended in M200 medium with 10% FBS were seeded in solidified Matrigel and incubated with test compounds for 6 h. The cells were then imaged.

2.7 *Apoptotic effect of* XCF-37b *on HUVEC and cancer cells*

To further determine whether the cytotoxic effect was attributable to the decreasing HUVEC viability, annexin-V/PI analysis was performed to detect apoptosis in VEGF-stimulated HUVECs in the presence of **XCF-37b**. Cells were treated with increasing concentrations of **XCF-37b** (1 μM, 5 μM, 10 μM, and 20 μM). As **Fig. 7** shows, **XCF-37b** did not significantly alter the VEGF effects on the percentage of apoptotic cells. We also detected the apoptotic protein marker PARP and caspase-3 after **XCF-37b** treatment using Western blot. No PARP or caspase-3 cleavage was observed with increasing concentrations of **XCF-37b**, suggesting that **XCF-37b** exerts antiproliferative activity without causing cytotoxic effects in HUVECs.

No apoptosis was observed after different concentrations of **XCF-37b** treatment (1 μM, 5 μM, 10 μM, and 20 μM) for 24 h. HT29 cells showed no apoptosis after **XCF-37b** (5 μM) exposure at 24, 48, and 72 h. Moreover, we observed no PARP or caspase-3 cleavage in the HT29 cells (**Fig. 8**).

No prominent apoptosis was observed after **XCF-37b** treatment in HUVEC or HT29 cells, indicating that the **XCF-37b**-induced inhibitions of cell proliferation, migration, and invasion were not cytotoxicity-related.

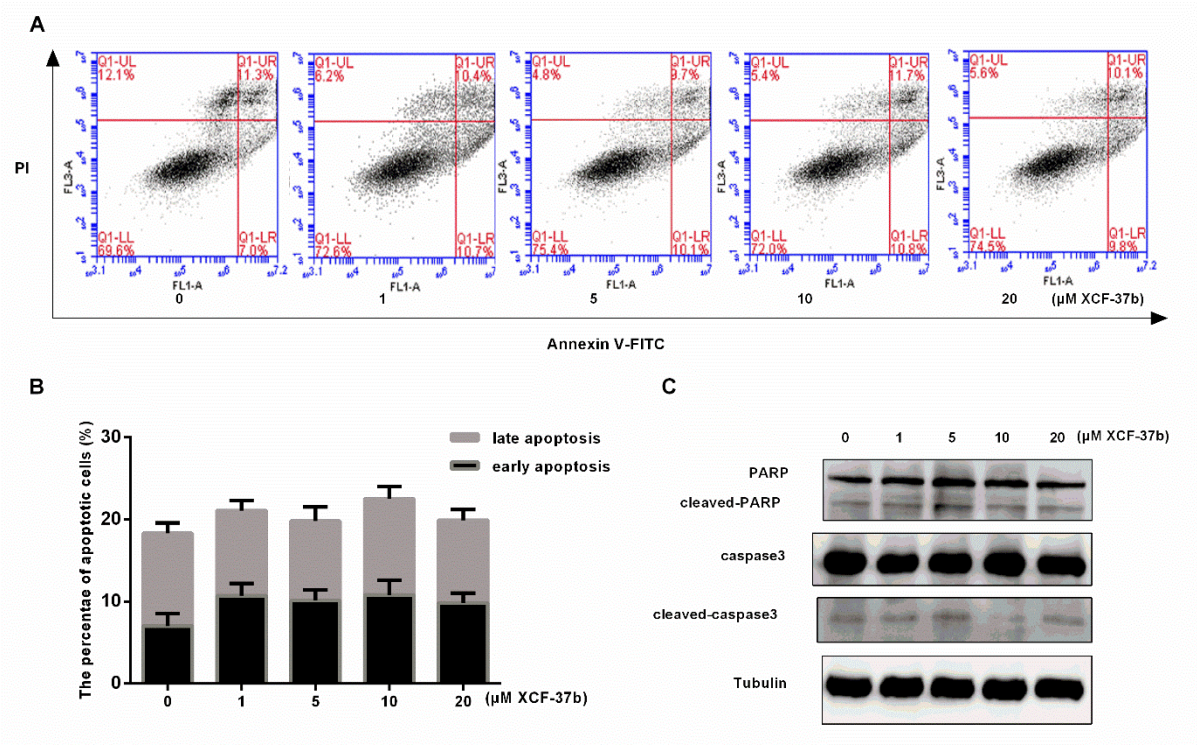

Fig. 7 Apoptosis of **XCF-37b** in HUVEC cells

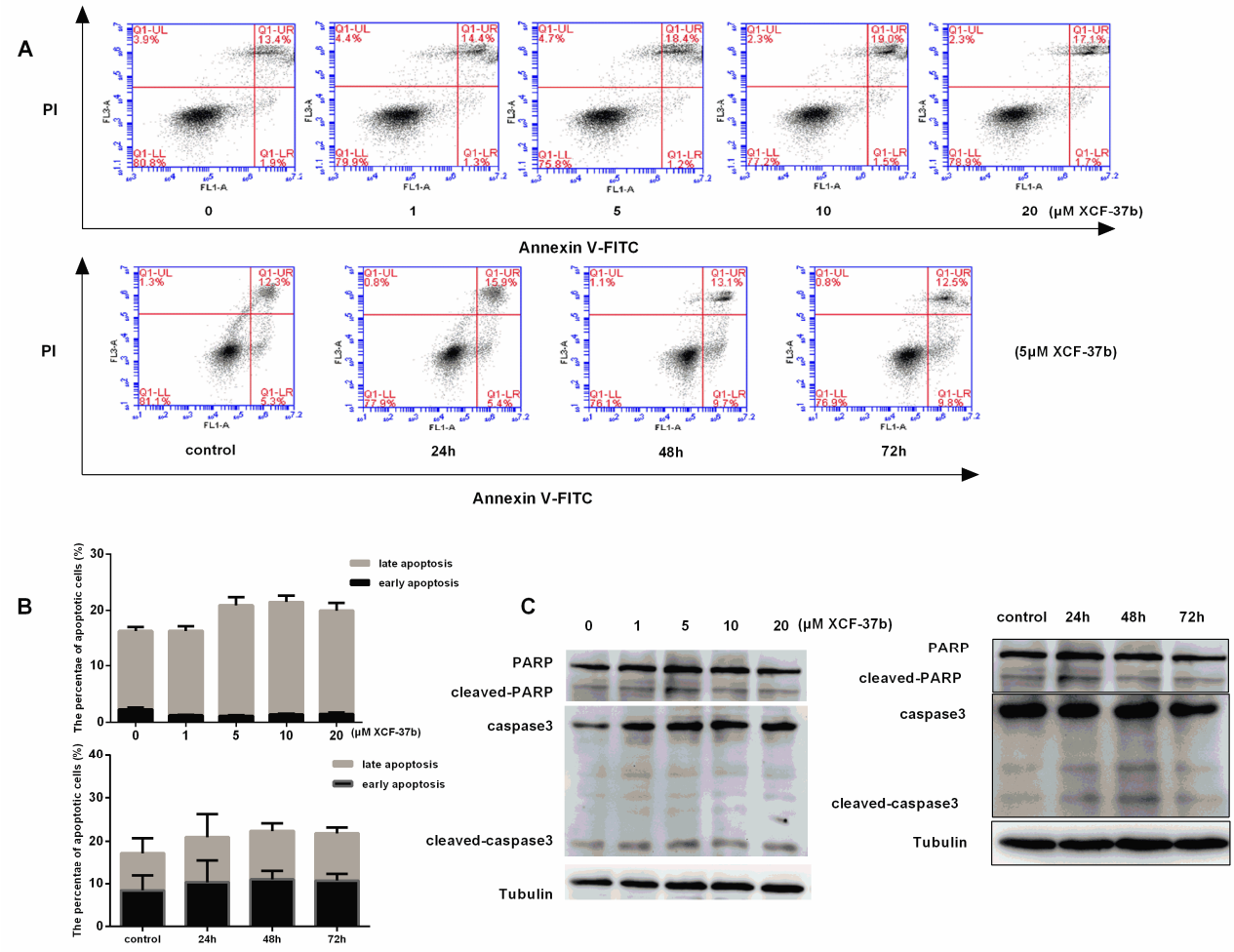

Fig. 8 Apoptosis of **XCF-37b** in HT29 cells

2.8 XCF-37b *attenuated the VEGFR2 signaling pathway in HUVEC cells*

VEGFR2 signaling is essential to vascular endothelial cell function. VEGFR2 binds with VEGF to phosphorylate VEGFR2, which then activates various downstream signaling cascades, such as MAPK/ERK, which is responsible for endothelial cell migration, proliferation, and survival. To understand the molecular mechanisms of **XCF-37b**-mediated antiangiogenic properties, we examined the pathways and signaling cascades using Western blot. As **Fig. 9a** shows, **XCF-37b** concentration-dependently suppressed VEGFR2 phosphorylation in VEGF-stimulated HUVECs. Dramatic downregulations of phospho-FAK (Tyr925), phospho-Src (Tyr416) phospho-AKT (Ser473) and phospho-ERK (Thr202/Tyr204), phospho-STAT3 (Tyr705), which are downstream targets of VEGFR2, were observed with 1, 5 and 10 μM of **XCF-37b** treatment. However, total FAK, Src, AKT, and ERK STAT3 remained unchanged **(Fig. 9a)**. The results revealed that **XCF-37b** inhibited angiogenesis by directly targeting VEGF-stimulated VEGFR2 activation in

endothelial cells and further suppressed VEGFR-2 downstream signaling pathways. AKT is a serine/threonine kinase that plays an important role in cell growth, proliferation, migration, protein synthesis, and angiogenesis. Activation of the AKT/mTOR/p70S6K pathway is required for endothelial cell proliferation and migration. Next, we examined expression of the AKT-mTOR signaling pathway after **XCF-37b** exposure and found that p-mTOR (Ser 2448) levels were reduced together with p-AKT. **XCF-37b** dose-dependently decreased the levels P70S6K (Thr389) in endothelial cells **(Fig. 9b**). These results showed that **XCF-37b** may inhibit endothelial cell proliferation by downregulating the AKT/mTOR/p70S6K pathway.

These studies demonstrated that **XCF-37b** is a potent inhibitor of tumor angiogenesis *in vitro* and *ex vivo*. **XCF-37b** inhibited VEGFR2 activation, thereby suppressing the AKT and ERK-mediated angiogenic signaling pathways.

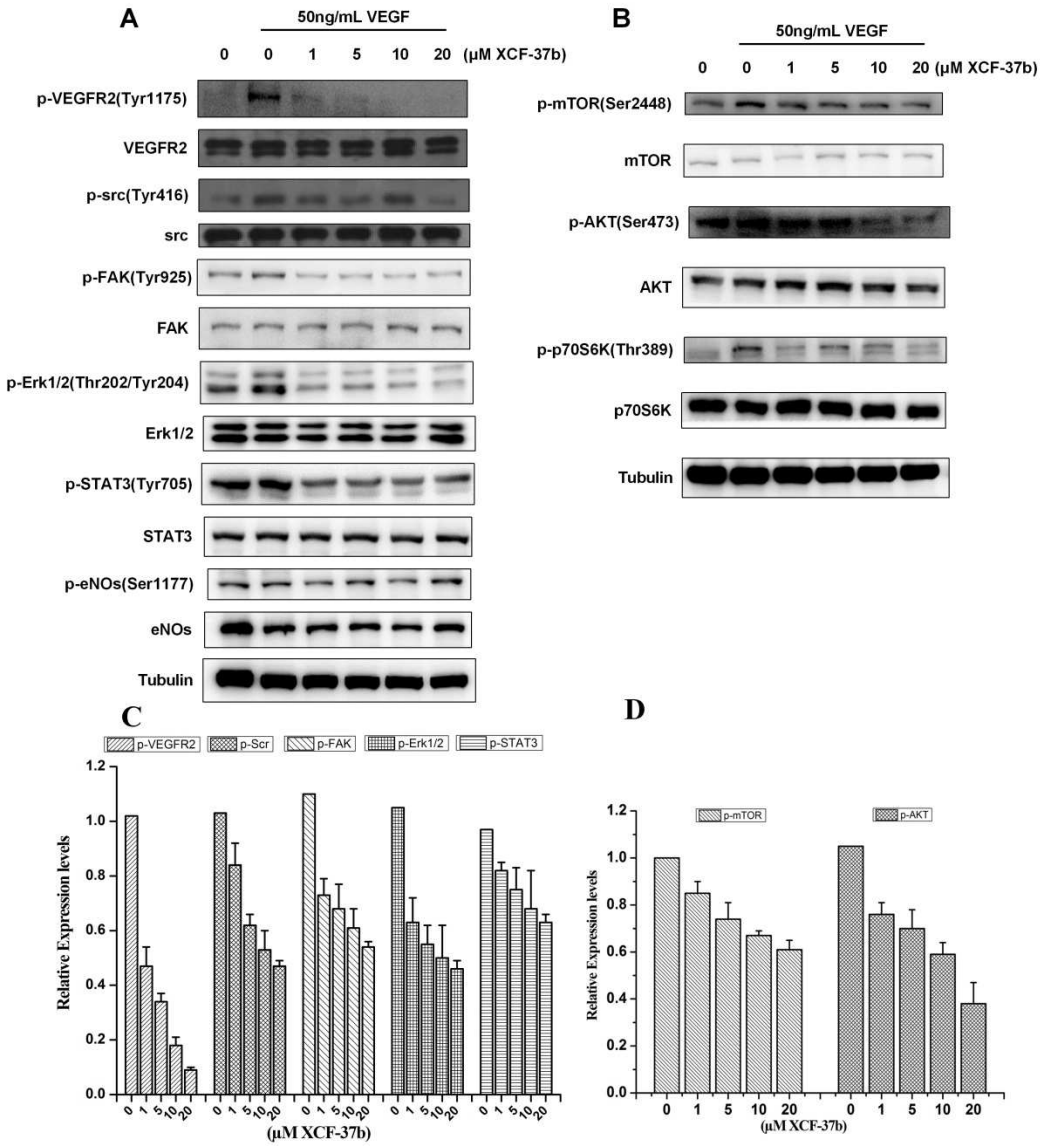

Fig. 9 XCF-37b inhibited VEGFR2 signaling pathways in HUVEC cells. The cells were starved overnight, then pretreated with the indicated concentrations of **XCF-37b** (1, 5, 10, and 20 μM) for 1.5 h, followed by the addition of VEGF (50 ng/mL) for another 30 min. Cell pellets were collected for immunoblotting. a) Effect of **XCF-37b** on VEGFR-2, Src, FAK, Erk1/1, and STAT3. b) Effect of **XCF-37b** on mTOR, AKT, and p70S6K. c, d, and e) Quantitative evaluation of enzymatic activities after **XCF-37b** treatment on gelatin zymography.

2.9 XCF-37b *blocked the AKT/mTOR/P70S6K pathway in HT 29 cells*

AKT, mTOR, and STAT3 phosphorylation was significantly dose-dependently reduced in HT29 cancer cells (**Fig. 10a**).

HIF-1α, a transcription factor, is consistently overexpressed in various cancer cells and is closely correlated with angiogenesis, tumor growth and metastasis[53]. VEGF is an HIF-1-responsive gene. HIF-1α binds to the hypoxia-responsive element of the VEGF promoter and activates VEGF gene expression at the transcriptional level[54]. VEGF and its family members are essential for inducing tumor angiogenesis, and aberrant expression of VEGF is a key regulator in hypoxia-induced angiogenesis[55]. Our study showed that inhibiting HIF activity reduced tumor growth. HIF-1α and VEGF were dramatically decreased when concentration-dependently treated with **XCF-37b** in HT29 cancer cells (**Fig. 10b**). HIF-1 is a key regulator of VEGF expression, suggesting that **XCF-37b** decreased VEGF expression via blocking the HIF-1 pathway. Additional RT-PCR analyses showed that **XCF-37b** did not reduce the VEGF mRNA levels; however, the HIF-1α mRNA level was reduced concentration-dependently.

Cancer cells secrete various angiogenic factors that change the adjacent endothelial cells and promote tumor angiogenesis, leading to tumor growth and progression[56, 57]. MMPs (especially MMP-2/9) degrade the extracellular matrix and are critical for cancer cell movement. **XCF-37b** treatment dose-dependently decreased the MMP-9 and MMP-2 expressions (**Fig. 10c**). Gelatin zymography examination revealed that **XCF-37b** treatment significantly reduced the secreted MMP 2/9 activity.

The data indicated that **XCF-37b** showed distinct antiangiogenic activity against tumor migration by downregulating MMP-9, MMP-2 activity, and the VEGF/HIF-1α signaling pathway.

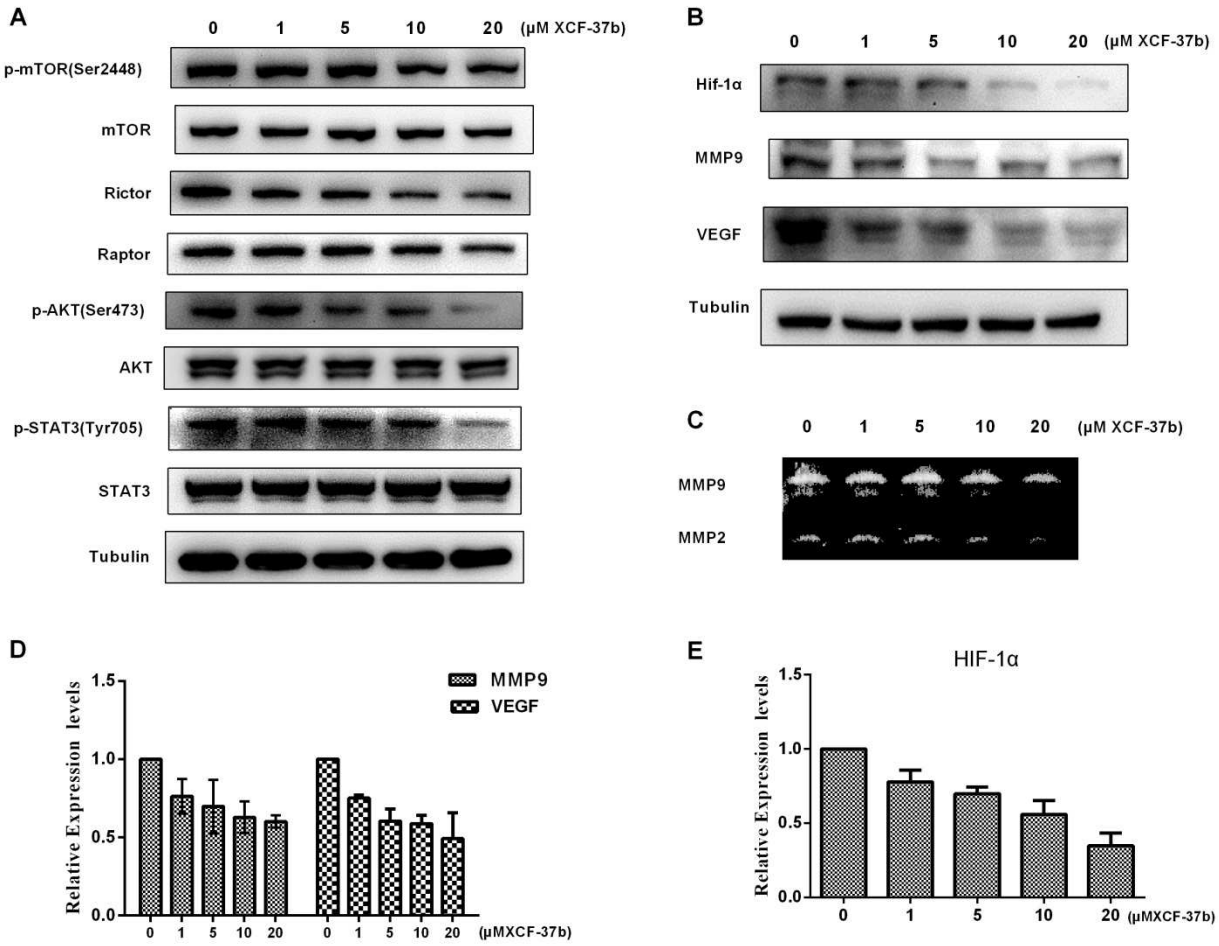

Fig. 10 XCF-37b inhibited VEGFR2 signaling pathways in HT29 cells. a) Effect of **XCF-37b** on AKT-mTOR signaling, HT29 cells were treated with the indicated concentrations of **XCF-37b** for 24 h, and cell lysates were subjected to immunoblotting. b) Effect of **XCF-37b** on HIF-α, VEGF and MMP-9. c) Effect of MMP-9 and MMP-2. d, e) Quantitative evaluation of MMP-9, VEGF and HIF-1α enzymatic activities after **XCF-37b** treatment on gelatin zymography.

2.10 *In vitro kinase screening for* XCF-37b

To investigate the potential protein target for the most active **XCF-37b** compound, **XCF-37b**'s kinase inhibitory profile was tested at 10 μM over a panel of 28 oncogenic kinases at Kebai Biotechnology Co., Ltd. (Nanjing, Jiangsu, China).[58] Fig. 11 shows that **XCF-37b** displayed good inhibitory activity (above 90%) against two kinases: VEGFR-2 (95.4%) and mTOR (93.8%). Moreover, it exerted moderate inhibitory activity (50–70%) towards AKT1, ERK1, ERK2 and P70S6K and modest activity against some other kinases with an inhibition percentage of <40%.

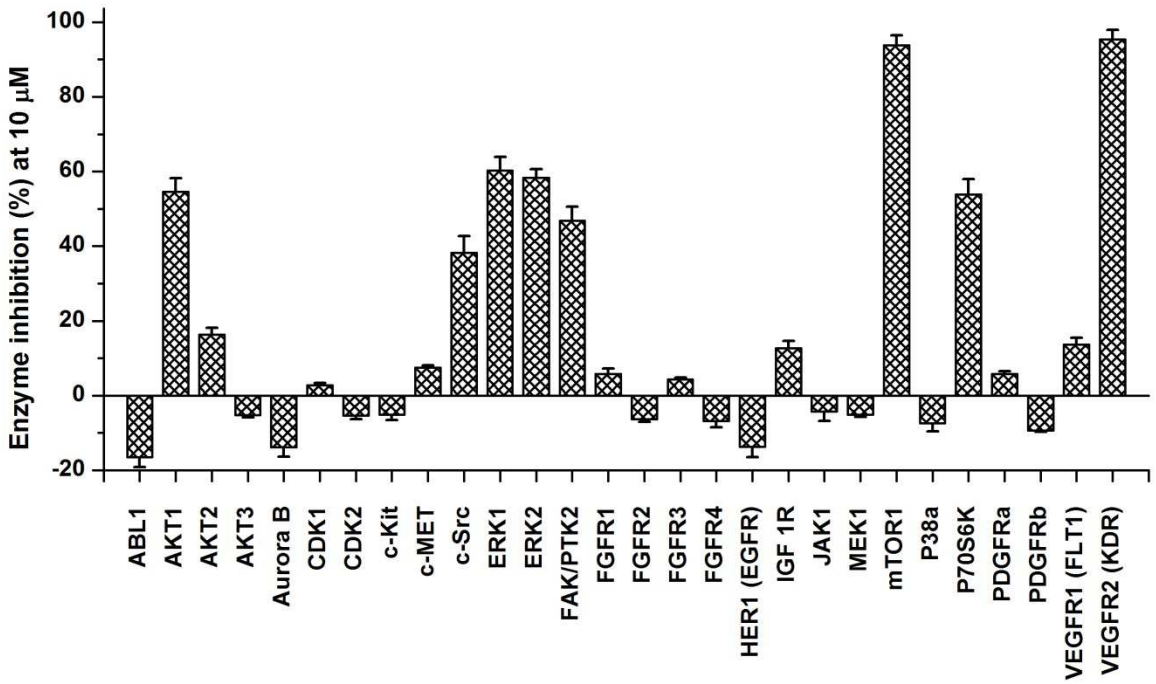

Fig. 11 Inhibition percentages of compound **XCF-37b** over 28 oncogenic kinases at 10 μM. Data are mean (± SD) for three independent experiments.

2.11 XCF-37b *inhibited tumor growth and angiogenesis in xenograft murine models*

To elucidate the antitumor effects of **XCF-37b** *in vivo*, HT29 colon xenograft murine models were used. **XCF-37b** was administered o.p. every other day for 3 weeks. The results showed that **XCF-37b** suppressed HT29 subcutaneous tumor growth (**Fig. 11**). The relative tumor volume in the **XCF-37b** group (60 mg/kg) was reduced by 53.51%. **XCF-37b** treatment did not significantly decrease the mouse body weight compared with that of the control. We further investigated the angiogenic effect in the tumor via staining with the CD31 endothelial marker. **XCF-37b** treatment markedly reduced the development of newly developed vessels in the tumors (**Fig. 12**). The mean vessel density in tumors treated with **XCF-37b** was reduced to 5%, which is similar to the effect of sunitinib. H&E staining showed that tumors exhibited large areas of late apoptotic and necrotic cells after **XCF-37b** treatment. Consistent with the *in vitro* results, the p-mTOR levels were reduced in the tumors after **XCF-37b** treatment. In addition, **XCF-37b** treatment reduced cell proliferation in tumors as shown by Ki-67 staining. **XCF-37b** treatment caused an apoptotic effect in tumors on the TUNEL assay. The results implied that **XCF-37b** suppressed tumorigenesis by targeting angiogenesis.

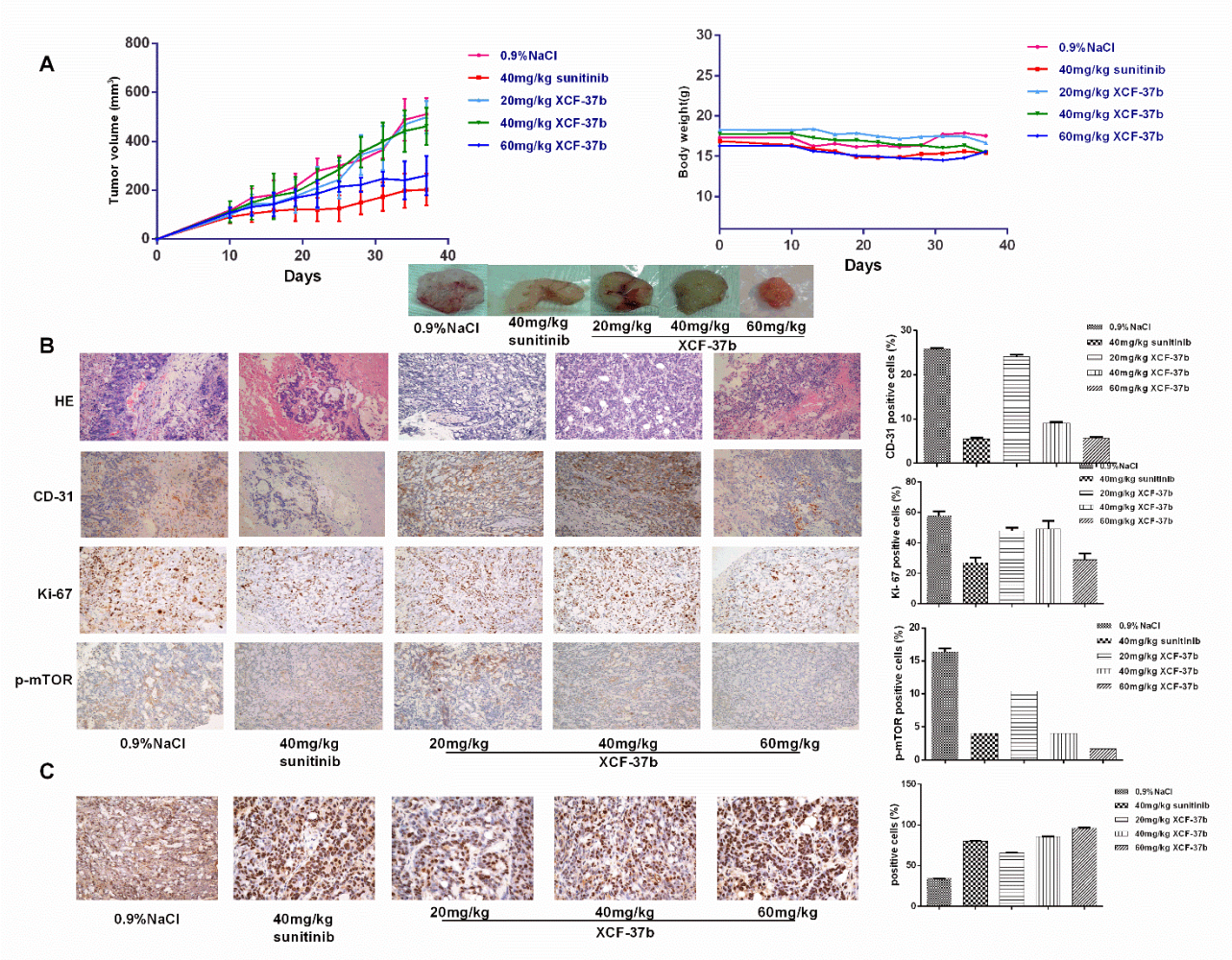

Fig. 12 XCF-37b inhibited tumor growth and neoangiogenesis in HT29 colon xenografts. a) *In vivo* tumor growth inhibition and body weight. b) Immunohistological assessments of H&E, CD-31, Ki-67, p-mTOR, and quantitative analysis; and c) Apoptotic effect of **XCF-37b** treatment in tumors via TUNEL assay

2.12 *Molecular docking study*

To rationalize the observed VEGFR-2 and mTOR kinase inhibitor activity from a three-dimensional (3D) structural perspective, **XCF-37b** was docked in the kinase domain using the GoldDock 5.0 module of Discovery Studio 3.5. **Fig. 13** illustrates the 3D-interaction model of **XCF-37b** with VEGFR-2 and mTOR, while Supplementary **Figs. 2S** and **3S** show the corresponding 2D interaction model. The docking model demonstrates that **XCF-37b** was located deep inside the extended hydrophobic pocket formed by the DFG out conformation of VEGFR-2 and the ATP-binding site of mTOR. The binding energies using the protocol (MM-PBSA-BINDING ENERGY) of **XCF-37b** inside VEGFR-2 and mTOR were -25.37 kJ/mol and -30.76 kJ/mol,

respectively. In VEGFR-2, two hydrogen-bonding interactions were observed: in the hinge region of the kinase, the amide oxygen of the benzamide moiety H-bonded to residue Lys868, and in the adenine region, the amide oxygen of the succinimide scaffold formed H-bonds with residue Cys919. Additionally, the N-phenyl ring of the succinimide was H-π stacked with residue Leu840, which enhanced the binding interaction to VEGFR-2 kinase. The para-methoxy of the benzamide moiety extended to a narrow hydrophobic subpocket of the allosteric site of VEGFR-2, which was embraced by residues Leu1019, Asp1046, and Leu889. In mTOR, two hydrogen-bonding interactions were observed: the amide oxygen of the benzamide moiety H-bonded to residue Val2240, and the amide oxygen of the succinimide scaffold formed H-bonds with residue Asp2357. Intriguingly, three H-π and one π-π interaction occurred between **XCF-37b** and mTOR kinase, in which N-phenyl rings of the succinimide stacked with Asp2357, a double bond stacked with Tyr2225, and the para-methoxy of the benzamide moiety stacked with Trp2239. These results indicated that compound **XCF-37b** is a dual inhibitor of VEGFR-2 and mTOR kinases.

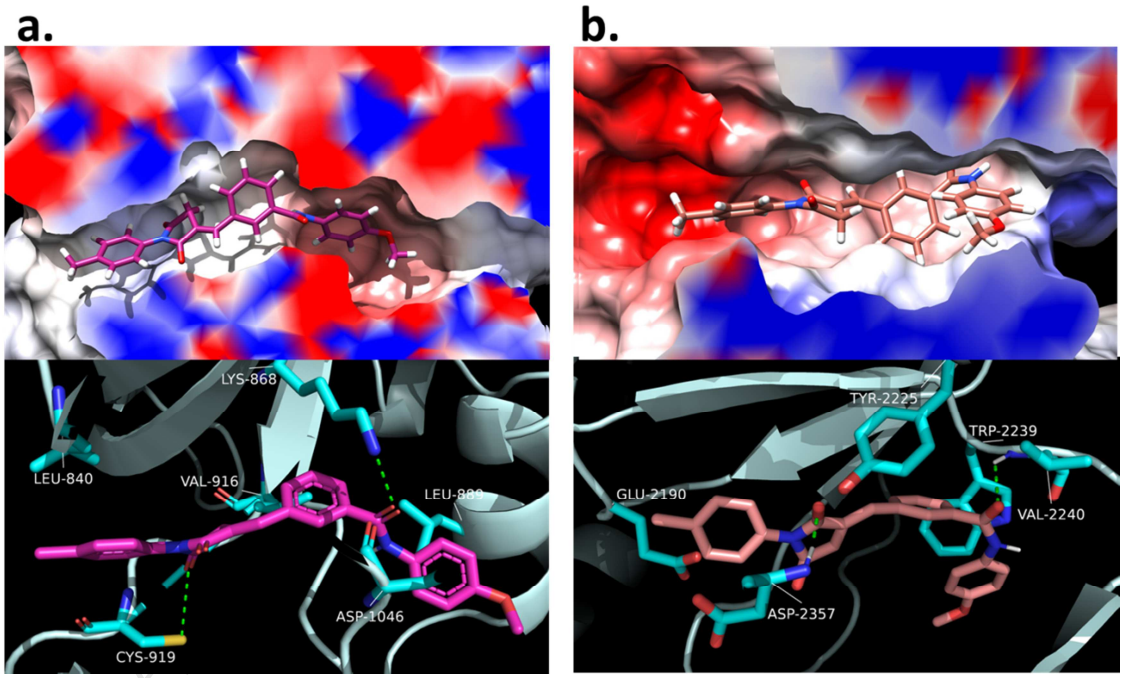

Fig. 13 Putative binding modes of compound **XCF-37b** in kinases were predicted by molecular modeling. The 3D images were prepared with Accelrys Discovery Studio, and the dashed lines illustrate atom pairs within hydrogen bonds; a) Binding mode of **XCF-37b** in VEGFR-2 kinase; b) Binding mode of **XCF-37b** in mTOR kinase.

3. Conclusions

In summary, a new class of benzylidene-succinimide derivatives was prepared and tested by

assessing its potential to inhibit angiogenesis. The biological evaluation identified several structurally distinct antiangiogenic inhibitors that caused no cytotoxic effects in HUVECs or HCT116, SW480 and NCM460 cancer cells. Among the series compounds, **XCF-37b** suppressed HUVEC migration and invasion and rat aortic ring angiogenesis *ex vivo*, possibly by suppressing angiogenesis-associated factors. **XCF-37b** inhibited HT29 colon tumor growth *in vivo*. This compound inhibited the AKT/mTOR and VEGFR2 signaling pathway, as evidenced by decreased expressions of phosphor-AKT (p-AKT), p-mTOR, p-VEGFR2 (Tyr175), p-Src (Tyr416), p-FAK (Tyr925), and p-Erk1/2 (Thr202/Tyr204). Moreover, **XCF-37b** significantly decreased the protein expressions of MMP-2, MMP-9 and HIF-1α. These results will help further optimize and develop new medication candidates for clinical studies as novel angiogenic inhibitors.

4. Experimental

4.1 *Chemistry*

All chemicals and reagents were of commercial grade and used without further purification. The reactions were monitored by thin-layer chromatography (TLC) using silica gel GF_{254}. Column chromatography was performed with 200–300 mesh silica gel. All yields refer to isolated products after purification. The intermediates and the products synthesized were fully characterized by spectroscopic data. The nuclear magnetic resonance (NMR) spectra were recorded with a Bruker DRX-500 NMR spectrometer (^{1}H: 500 MHz, ^{13}C: 125 MHz) using $CDCl_3$ or DMSO-d_6 as solvents. Chemical shifts (δ) are expressed in parts per million (ppm), and J values are given in hertz (Hz). IR spectra were recorded with a Fourier transform-infrared (FT-IR) Thermo Nicolet Avatar 360 spectroscope using a KBr pellet. High-resolution mass spectrometry (HRMS) was performed by liquid chromatography/mass selective detector time-of-flight (LC/MSD TOF) using an Agilent instrument. The melting points were measured using an XT-4A melting point apparatus without correction.

4.1.1 Synthesis of N-substituted phenyl maleimide

Maleic anhydride (0.05 mol) was dissolved in 0.2 mol ethyl acetate and stirred in an ice bath. After the maleic anhydride completely dissolved, 0.05 mol substituted aniline (compounds **a**) was added to 0.2 mol ethyl acetate solution. The yellow solid was slowly precipitated in the reaction. After stirring for 1 h in an ice bath, the resultant solution was filtered and washed. N-substituted phenyl maleamic acid was obtained with a yield over 97%. Next, 0.05 mol maleamic acid was

dissolved in 0.2 mol acetic anhydride while adding 0.025 mol of triethylamine. The solution was heated and stirred in an oil bath at 55–65°C for 1 hour. When the reaction cooled, the resultant solution was added to isovolumetric deionized water and left to stand overnight. The precipitated yellow solid was filtered and washed. N-substituted phenyl maleimide was obtained with a yield of over 88%.

4.1.2 Synthesis of N-butyl maleimide and N-benzyl maleimide

Maleic anhydride (60 g; 0.61 mol) and 90 mL acetone were mixed in a 500-mL four-port bottle. A mixture of butylamine 57 mL (0.58 mol) or benzylamine 64 mL (0.58 mol) in acetone 90 mL was then added slowly into the solution under nitrogenous conditions and rapidly agitated. After the titration was complete, the reaction was stirred for 1 h. Next, 85 mL of acetic anhydride, 36 mL of triethylamine, and 1.8 mL of 1:6 nickel sulfate aqueous solution were added to the reaction system. The reaction temperature was raised to 70°C, and the reflux reaction lasted 4 hours. After cooling to room temperature, the reactants were washed to near neutral using water, saturated Na_2CO_3 solution and water again. After drying and distillation, the product yield was over 88%.

4.1.3 General procedure for synthesizing N-substituted benzylidene pyrrolidine dione derivatives (compounds **f***)*

N-substituted maleimide (0.014 mol; compound **d**) was dissolved in 40 mL alcohol and stirred. After N-substituted maleimide was completely dissolved, 0.012 mol triphenylphosphine was added to the reaction for 4–5 minutes. Next, 3-carboxybenzaldehyde (0.01 mol) was added rapidly and stirred at room temperature for 6 hours. White solids were precipitated, filtered and washed. The product was obtained, and the yield was over 90%.

4.1.4 General procedure for synthesizing benzylidene-succinimide derivatives (compounds **g1-g33***)*

N-substituted benzylidene pyrrolidine dione (0.5 mol), 0.6 mmol TBTU, and 0.6 mmol EDCI were dissolved in 2 mL DCM and 0.75 mmol DIEA mixture solution and stirred for 30 minutes. Next, 0.5 mol of amine or methylamino acid in DCM (8 mL) solution was slowly added to the solution and stirred at room temperature for 4–10 hours with the TLC monitoring reaction. After the reaction was

complete, the resultant solution was washed with dilute hydrochloric acid and saturated sodium bicarbonate solution, then dried with anhydrous sodium sulfate, followed by column chromatography separation. The target product was obtained by crystallization. The yield ranged from 72–90%.

4.1.5 Spectral data of compounds g1-g33

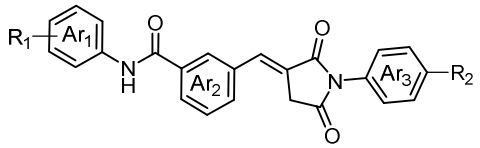

General structure for **g1-g33**

3-((2,5-Dioxo-1-phenylpyrrolidin-3-ylidene)methyl)-N-phenylbenzamide (g1)

Yellow solid; M.p. 231-232 °C; **^{1}H NMR** (500 MHz, DMSO-d_6) δ = 10.38 (s, 1H, HN), 8.23 (s, 1H, HAr_2), 8.03 (d, J = 8.1 Hz, 1H, HAr_2), 7.94 (d, J = 7.8 Hz, 1H, HAr_2), 7.82 (d, J = 7.2 Hz, 2H, HAr), 7.73 – 7.63 (m, 2H, HAr and C=CH), 7.54 (t, J = 7.6 Hz, 2H, HAr), 7.46 (t, J = 7.4 Hz, 1H, HAr), 7.43 – 7.34 (m, 4H, HAr), 7.14 (t, J = 7.4 Hz, 1H, HAr), 3.98 (d, J = 2.4 Hz, 2H, CH_2). **^{13}C NMR** (126 MHz, DMSO-d_6) δ = 173.77, 170.22, 165.41, 139.42, 136.16, 134.61, 133.28, 132.95, 132.24, 129.75, 129.62, 129.40, 129.21, 129.05, 128.66, 127.50, 126.76, 124.23, 120.84, 34.45; **HRMS** (TOF ESI$^+$): m/z calcd for $C_{24}H_{18}N_2O_3$ $[M+Na]^+$, 405.1210, found, 405.1211.

3-((2,5-Dioxo-1-phenylpyrrolidin-3-ylidene)methyl)-N-(4-fluorophenyl)benzamide (g2)

Yellow solid; M.p. 235-236 °C; **^{1}H NMR** (500 MHz, DMSO-d_6) δ = 10.43 (s, 1H, HN), 8.22 (d, J = 2.1 Hz, 1H, HAr_2), 8.03 (d, J = 7.7 Hz, 1H, HAr_2), 7.93 (d, J = 7.8 Hz, 1H, HAr_2), 7.87 – 7.79 (m, 2H, HAr), 7.72 – 7.64 (m, 2H, HAr and C=CH), 7.54 (t, J = 7.6 Hz, 2H, HAr), 7.49 – 7.43 (m, 1H, HAr), 7.40 (dd, J = 7.8, 1.6 Hz, 2H, HAr), 7.28 – 7.18 (m, 2H, HAr), 3.98 (d, J = 2.4 Hz, 2H, CH_2); **^{13}C NMR** (125 MHz, DMSO-*d6*): δ = 173.72, 170.17, 165.32, 159.76, 157.85, 135.99, 135.76, 134.63, 133.29, 132.23, 129.70, 129.62, 129.35, 129.19, 128.64, 127.47, 126.77, 122.74, 122.68, 115.69, 115.52, 34.44; **HRMS** (TOF ESI$^+$): m/z calcd for $C_{24}H_{17}FN_2O_3$ $[M+Na]^+$, 423.1115, found, 423.1115.

3-((2,5-Dioxo-1-phenylpyrrolidin-3-ylidene)methyl)-N-p-tolylbenzamide (g3)

Yellow solid; M.p. 231-232 °C; **^{1}H NMR** (500 MHz, DMSO-d_6) δ = 10.29 (s, 1H, HN), 8.21 (s, 1H, HAr_2), 8.02 (d, J = 8.1 Hz, 1H, HAr_2), 7.92 (d, J = 8.2 Hz, 1H, HAr_2), 7.70 – 7.65 (m, , 4H, $HAr_{3,2}$ and C=CH), 7.54 (t, J = 7.7 Hz, 2H, HAr_3), 7.46 (t, J = 7.4 Hz, 1H, HAr_3), 7.40 (d, J = 8.1 Hz, 2H,

HAr_1), 7.19 (d, J = 8.2 Hz, 2H, HAr_1), 3.97 (d, J = 2.4 Hz, 2H, CH_2), 2.30 (s, 3H, CH_3); **^{13}C NMR** (126 MHz, DMSO-d_6) δ = 173.77, 170.21, 165.17, 136.87, 136.20, 134.58, 133.21, 132.94, 132.24, 129.68, 129.60, 129.43, 129.35, 129.21, 128.66, 127.49, 126.72, 120.86, 34.44, 20.89; **HRMS** (TOF ESI$^+$): m/z calcd for $C_{25}H_{20}N_2O_3$ $[M+Na]^+$, 419.1366, found, 419.1366.

3-((2,5-Dioxo-1-phenylpyrrolidin-3-ylidene)methyl)-N-(4-methoxyphenyl)benzamide (g4)

Yellow solid; M.p. 231-232 °C; **^{1}H NMR** (500 MHz, DMSO-d_6) δ = 10.16 (s, 1H, HN), 8.13 (s, 1H, HAr_2), 7.93 (d, J = 7.7 Hz, 1H, HAr_2), 7.83 (d, J = 7.8 Hz, 1H, HAr_2), 7.63 (d, J = 8.9 Hz, 2H, HAr_1), 7.59 – 7.56 (m, 2H, HAr_2 and C=CH), 7.45 (t, J = 7.5 Hz, 2H, HAr_3), 7.38 (d, J = 7.8 Hz, 1H, HAr_3), 7.31 (d, J = 7.6 Hz, 2H, HAr_3), 6.88 (d, J = 9.0 Hz, 2H, HAr_1), 3.89 (d, J = 2.5 Hz, 2H, CH_2), 3.68 (s, 3H, OCH_3); **^{13}C NMR** (126 MHz, DMSO-d_6) δ = 174.24, 170.69, 165.43, 156.58, 136.70, 135.07, 133.63, 133.45, 132.94, 132.77, 130.09, 129.80, 129.70, 129.14, 127.98, 127.19, 122.97, 114.67, 56.07, 34.95; **HRMS** (TOF ESI$^+$): m/z calcd for $C_{25}H_{20}N_2O_4$ $[M+Na]^+$, 435.1315, found, 435.1317.

1-phenyl-3-(3-(pyrrolidine-1-carbonyl)benzylidene)pyrrolidine-2,5-dione (g5)

Yellow solid; M.p. 210-212 °C; **^{1}H NMR** (500 MHz, Chloroform-d) δ = 7.66 (t, J = 2.5 Hz, 1H, HAr_2), 7.61 (s, 1H, HAr_2), 7.51 (t, J = 7.1 Hz, 2H, HAr), 7.48 – 7.39 (m, 3H, HAr, C=CH), 7.35 (d, J = 7.6 Hz, 1H, HAr), 7.31 (dd, J = 8.4, 1.3 Hz, 2H, HAr), 3.71 (d, J = 2.4 Hz, 2H, $COCH_2$), 3.60 (t, J = 7.0 Hz, 2H, NCH_α), 3.37 (t, J = 6.6 Hz, 2H, NCH_β), 1.99 – 1.89 (m, 2H, $CH_{2\alpha}CH_{2\alpha}$), 1.85 (q, J = 6.5 Hz, 2H, $CH_{2\beta}CH_{2\beta}$); **^{13}C NMR** (126 MHz, Chloroform-d) δ = 173.16, 170.19, 168.99, 138.71, 134.89, 134.59, 132.33, 131.81, 129.57, 129.23, 129.06, 126.83, 124.51, 50.07, 46.74, 34.66, 26.85, 24.83; **HRMS** (TOF ESI$^+$): m/z calcd for $C_{22}H_{20}N_2O_3$ $[M+Na]^+$, 383.1366, found, 383.1367.

3-(3-(morpholine-4-carbonyl)benzylidene)-1-phenylpyrrolidine-2,5-dione (g6)

Yellow solid; M.p. 218-220 °C; **^{1}H NMR** (500 MHz, Chloroform-d) δ = 7.65 (s, 1H, HAr_2), 7.56 – 7.48 (m, 2H, HAr), 7.47 – 7.38 (m, 4H, HAr and C=CH), 7.34 (t, J = 7.4 Hz, 1H, HAr), 7.30 (d, J = 7.9 Hz, 2H, HAr), 3.69 (d, J = 2.6 Hz, 2H, $COCH_2$), 1.21 (ddd, J = 14.6, 9.3, 5.5 Hz, 4H, CH_2OCH_2), 0.81 (qd, J = 11.8, 9.6, 4.0 Hz, 4H, CH_2NCH_2); **^{13}C NMR** (126 MHz, Chloroform-d) δ = 172.53, 169.60, 169.25, 136.41, 134.54, 134.02, 131.18, 129.38, 129.09, 128.72, 128.57, 126.33, 124.47, 66.78, 34.15; **HRMS** (TOF ESI$^+$): m/z calcd for $C_{22}H_{20}N_2O_4$ $[M+Na]^+$, 399.1315, found, 399.1317.

N-Benzyl-3-((2,5-dioxo-1-phenylpyrrolidin-3-ylidene)methyl)benzamide (g7)

Yellow solid; M.p. 231-232 °C; **^{1}H NMR** (500 MHz, DMSO-d_6) δ = 9.20 (t, J = 6.0 Hz, 1H, HN), 8.17 (s, 1H, HAr_2), 7.99 (d, J = 8.0 Hz, 1H, HAr_2), 7.89 (d, J = 8.1 Hz, 1H, HAr_2), 7.64 – 7.61 (m, 2H, HAr and C=CH), 7.54 (t, J = 7.7 Hz, 2H, HAr), 7.46 (d, J = 7.5 Hz, 1H, HAr), 7.41 – 7.34 (m, 6H, HAr), 7.29 – 7.25 (m, 1H, HAr), 4.55 (d, J = 5.9 Hz, 2H, CH_2Ar_1), 3.96 (d, J = 2.4 Hz, 2H, $COCH_2$); **^{13}C NMR** (126 MHz, DMSO-d_6) δ = 173.78, 170.20, 166.06, 139.89, 135.47, 134.59, 133.28, 132.95, 132.27, 129.61, 129.20, 129.13, 129.00, 128.70, 127.62, 127.49, 127.18, 126.65, 43.12, 34.45; **HRMS** (TOF ESI$^+$): m/z calcd for $C_{25}H_{20}N_2O_3$ $[M+Na]^+$, 419.1366,found, 419.1363.

N-cyclohexyl-3-((2,5-dioxo-1-phenylpyrrolidin-3-ylidene)methyl)benzamide (g8)

Yellow solid; M.p. 201-203 °C; **^{1}H NMR** (500 MHz, DMSO-d_6) δ = 8.32 (d, J = 7.9 Hz, 1H, HN), 8.11 (d, J = 2.2 Hz, 1H, HAr_2), 7.93 (d, J = 7.8 Hz, 1H, HAr_2), 7.85 (d, J = 7.8 Hz, 1H, HAr_2), 7.64 – 7.58 (m, 2H, HAr and C=CH), 7.54 (t, J = 7.7 Hz, 2H, HAr_3), 7.46 (d, J = 7.5 Hz, 1H, HAr), 7.41 – 7.36 (m, 2H, HAr_3), 3.93 (d, J = 2.5 Hz, 2H, $COCH_2$), 3.86 – 3.77 (m, 1H, CHN), 1.87 (d, J = 8.9 Hz, 2H, CH_2), 1.76 (d, J = 9.5 Hz, 2H, CH_2), 1.63 (d, J = 13.0 Hz, 1H, CH_2) 1.34 (q, J = 11.0 Hz, 4H, CH_2), 1.20 – 1.13 (m, 1H, CH_2); **^{13}C NMR** (126 MHz, DMSO-d_6) δ = 173.76, 170.21, 165.16, 135.97, 134.40, 132.95, 132.64, 132.38, 129.50, 129.40, 129.19, 129.09, 128.63, 127.48, 126.44, 48.88, 34.41, 32.81, 25.66, 25.31; **HRMS** (TOF ESI$^+$): m/z calcd for $C_{24}H_{24}N_2O_3$ $[M+Na]^+$, 411.1679, found, 411.1677.

N-(4-Chlorophenyl)-3-((2,5-dioxo-1-phenylpyrrolidin-3-ylidene)methyl)benzamide (g9)

Yellow solid; M.p. 233-234 °C; **^{1}H NMR** (500 MHz, DMSO-d_6) δ = 10.49 (s, 1H, HN), 8.21 (s, 1H, HAr_2), 8.02 (d, J = 7.9 Hz, 1H, HAr_2), 7.97 – 7.91 (m, 1H, HAr_2), 7.85 (d, J = 8.9 Hz, 2H, HAr_1), 7.70 – 7.65 (m, 2H, HAr_3 and C=CH), 7.54 (dd, J = 8.2, 7.0 Hz, 2H, HAr_3), 7.48 – 7.43 (m, 3H, HAr), 7.40 (dd, J = 8.4, 1.3 Hz, 2H, HAr), 3.97 (d, J = 2.5 Hz, 2H, CH_2); **^{13}C NMR** (126 MHz, DMSO-d_6) δ = 173.74, 170.19, 165.52, 138.39, 135.89, 134.63, 133.39, 132.94, 132.16, 129.77, 129.65, 129.39, 129.21, 128.96, 128.66, 127.85, 127.48, 126.82, 122.31, 34.44; **HRMS** (TOF ESI$^+$): m/z calcd for $C_{24}H_{17}ClN_2O_3$ $[M+Na]^+$, 439.0819, found, 439.0817.

3-((2,5-Dioxo-1-phenylpyrrolidin-3-ylidene)methyl)-N-(3-fluorophenyl)benzamide (g10)

Yellow solid; M.p. 224-225 °C; **^{1}H NMR** (500 MHz, DMSO-d_6) δ = 10.51 (s, 1H, HN), 8.14 (s, 1H, HAr_2), 7.94 (d, J = 7.7 Hz, 1H, HAr_2), 7.85 (d, J = 7.8 Hz, 1H, HAr_2), 7.72 (dt, J = 11.7, 2.3 Hz, 1H, HAr), 7.62 – 7.55 (m, 2H, HAr and C=CH), 7.52 (dd, J = 8.1, 1.9 Hz, 1H, HAr), 7.45 (t, J = 7.6 Hz,

2H, HAr), 7.39 – 7.29 (m, 4H, HAr), 6.88 (td, *J* = 8.5, 2.7 Hz, 1H, HAr), 3.89 (d, *J* = 2.4 Hz, 2H, CH_2); **^{13}C NMR** (125MHz, DMSO-d_6): δ = 173.73, 170.17, 165.70, 163.42, 161.50, 141.26, 141.18, 135.81, 134.64, 133.45, 132.94, 132.16, 130.67, 130.59, 129.81, 129.64, 129.41, 129.20, 128.64, 127.47, 126.83, 116.45, 110.72, 110.55, 107.56, 107.35, 34.44; **HRMS** (TOF ESI$^+$): m/z calcd for $C_{24}H_{17}FN_2O_3$ [M+Na]$^+$, 423.1115, found, 423.1116.

3-((2,5-Dioxo-1-phenylpyrrolidin-3-ylidene)methyl)-N-m-tolylbenzamide (g11)

Yellow solid; M.p. 225-226 °C; **^{1}H NMR** (500 MHz, DMSO-d_6) δ = 10.29 (s, 1H, HN), 8.22 (s, 1H, HAr_2), 8.03 (d, *J* = 7.8 Hz, 1H, HAr_2), 7.93 (d, *J* = 7.8 Hz, 1H, HAr_2), 7.69 – 7.66 (m, 3H, HAr and C=CH), 7.62 (d, *J* = 8.1 Hz, 1H, HAr), 7.54 (t, *J* = 7.6 Hz, 2H, HAr), 7.47 (d, *J* = 7.4 Hz, 1H, HAr), 7.40 (d, *J* = 7.8 Hz, 2H, HAr), 7.27 (t, *J* = 7.8 Hz, 1H, HAr), 6.96 (d, *J* = 7.5 Hz, 1H, HAr), 3.97 (d, *J* = 2.4 Hz, 2H, CH_2), 2.34 (s, 3H, CH_3); **^{13}C NMR** (126 MHz, DMSO-d_6) δ = 173.76, 170.21, 165.31, 139.33, 138.21, 136.17, 134.59, 133.26, 132.95, 132.24, 129.69, 129.61, 129.38, 129.21, 128.87, 128.66, 127.49, 126.73, 124.93, 121.37, 118.02, 34.44, 21.59; **HRMS** (TOF ESI$^+$): m/z calcd for $C_{25}H_{20}N_2O_3$ [M+Na]$^+$, 419.1366, found, 419.1364.

N-(3,4-Dimethylphenyl)-3-((2,5-dioxo-1-phenylpyrrolidin-3-ylidene)methyl)benzamide (g12)

Yellow solid; M.p. 224-225 °C; **^{1}H NMR** (500 MHz, DMSO-d_6) δ = 10.21 (s, 1H, HN), 8.21 (s, 1H, HAr_2), 8.02 (d, *J* = 7.3 Hz, 1H, HAr_2), 7.91 (d, *J* = 7.8 Hz, 1H, HAr_2), 7.70 – 7.63 (m, 2H, HAr and C=CH), 7.59 (s, 1H, HAr), 7.53 (d, *J* = 7.2 Hz, 3H, HAr), 7.49 – 7.43 (m, 1H, HAr), 7.40 (d, *J* = 8.1 Hz, 2H, HAr), 7.13 (d, *J* = 8.3 Hz, 1H, HAr), 3.97 (s, 2H, CH_2), 2.24 (s, 3H, CH_3), 2.21 (s, 3H, CH_3); **^{13}C NMR** (126 MHz, DMSO-d_6) δ = 173.75, 170.20, 165.05, 137.09, 136.60, 136.19, 134.56, 133.17, 132.94, 132.26, 132.01, 129.88, 129.64, 129.57, 129.34, 129.20, 128.65, 127.48, 126.68, 122.09, 118.40, 34.43, 20.01, 19.22; **HRMS** (TOF ESI$^+$): m/z calcd for $C_{26}H_{22}N_2O_3$ [M+Na]$^+$, 433.1523, found, 433.1520.

3-((2,5-Dioxo-1-phenylpyrrolidin-3-ylidene)methyl)-N-(4-ethoxyphenyl)benzamide (g13)

Yellow solid; M.p. 195-196 °C; **^{1}H NMR** (500 MHz, DMSO-d_6) δ = 10.24 (s, 1H, HN), 8.21 (s, 1H, HAr_2), 8.02 (d, *J* = 8.2 Hz, 1H, HAr_2), 7.92 (d, *J* = 7.8 Hz, 1H, HAr_2), 7.71 – 7.64 (m, 4H, HAr and C=CH), 7.54 (t, *J* = 7.7 Hz, 2H, HAr), 7.46 (t, *J* = 7.4 Hz, 1H, HAr), 7.40 (d, *J* = 7.1 Hz, 2H, HAr), 6.95 (d, *J* = 9.0 Hz, 2H, HAr_1), 4.02 (q, *J* = 7.0 Hz, 2H, $COCH_2$), 3.97 (d, *J* = 2.4 Hz, 2H, OCH_2), 1.34 (t, *J* = 7.0 Hz, 3H, CH_3); **^{13}C NMR** (126 MHz, DMSO-d_6) δ = 173.77, 170.21, 164.93, 155.34, 136.22, 134.57, 133.15, 132.94, 132.31, 129.60, 129.31, 129.20, 128.65, 127.49, 126.68, 122.46,

114.69, 63.49, 34.44, 15.07; **HRMS** (TOF ESI$^+$): m/z calcd for $C_{26}H_{22}N_2O_4$ [M+Na]$^+$, 449.1472, found, 449.1474.

3-((2,5-dioxo-1-phenylpyrrolidin-3-ylidene)methyl)-N-(3,4,5-trimethoxyphenyl)benzamide (g14)

Yellow solid; M.p. 213-215 °C; **^{1}H NMR** (500 MHz, DMSO-d_6) δ = 10.43 (s, 1H, HN), 8.28 (s, 1H, HAr_2), 8.06 (d, J = 7.8 Hz, 1H, HAr_2), 7.92 (d, J = 7.8 Hz, 1H, HAr_2), 7.70 – 7.63 (m, 2H, HAr and C=CH), 7.54 (t, J = 7.6 Hz, 2H, HAr), 7.46 (d, J = 7.3 Hz, 1H, HAr), 7.39 (d, J = 7.8 Hz, 2H, HAr), 7.33 (s, 2H, HAr), 4.00 (d, J = 2.5 Hz, 2H, CH_2), 3.79 (s, 6H, OCH_3), 3.66 (s, 3H, OCH_3); **^{13}C NMR** (126 MHz, DMSO-d_6) δ = 173.76, 170.19, 165.17, 152.99, 136.02, 135.61, 134.57, 133.30, 132.94, 132.27, 129.71, 129.56, 129.34, 129.21, 128.65, 127.48, 126.72, 98.71, 60.51, 56.17, 34.49; **HRMS** (TOF ESI$^+$): m/z calcd for $C_{27}H_{24}N_2O_6$ [M+Na]$^+$, 495.1527, found, 495.1527.

3-((2,5-dioxo-1-phenylpyrrolidin-3-ylidene)methyl)-N-(3-(methylthio)phenyl)benzamide (g15)

Yellow solid; M.p. 234-236 °C; **^{1}H NMR** (500 MHz, DMSO-d_6) δ = 10.37 (s, 1H, HN), 8.22 (d, J = 2.1 Hz, 1H, HAr_2), 8.02 (d, J = 8.0 Hz, 1H, HAr_2), 7.94 (d, J = 7.8 Hz, 1H, HAr_2), 7.79 (d, J = 2.2 Hz, 1H, C=CH), 7.70 – 7.65 (m, 2H, HAr), 7.61 (d, J = 7.9 Hz, 1H, HAr), 7.58 – 7.51 (m, 2H, HAr), 7.46 (t, J = 7.4 Hz, 1H, HAr), 7.40 (d, J = 8.1 Hz, 2H, HAr), 7.33 (t, J = 8.0 Hz, 1H, HAr), 7.03 (d, J = 7.8 Hz, 1H, HAr), 3.97 (s, 2H, CH_2), 2.50 (s, 3H, SCH_3); **^{13}C NMR** (126 MHz, DMSO-d_6) δ = 173.74, 170.19, 165.48, 139.97, 138.92, 136.00, 134.63, 133.32, 132.94, 132.20, 129.77, 129.63, 129.56, 129.36, 129.21, 128.66, 127.49, 126.79, 121.63, 117.88, 117.25, 34.44, 15.09; **HRMS** (TOF ESI$^+$): m/z calcd for $C_{25}H_{20}N_2O_3S$ [M+Na]$^+$, 451.1087, found, 451.1085.

N-(2,5-dimethoxyphenyl)-3-((2,5-dioxo-1-phenylpyrrolidin-3-ylidene)methyl)benzamide (g16)

Yellow solid; M.p. 246-248 °C; **^{1}H NMR** (500 MHz, DMSO-d_6) δ = 9.58 (s, 1H, HN), 8.22 (s, 1H, HAr_2), 8.01 (d, J = 7.8 Hz, 1H, HAr_2), 7.92 (d, J = 8.1 Hz, 1H, HAr_2), 7.67 – 7.51 (m, 2H, HAr and C=CH), 7.57 – 7.51 (m, 3H, HAr), 7.46 (d, J = 7.5 Hz, 1H, HAr), 7.39 (d, J = 7.0 Hz, 2H, HAr), 7.03 (d, J = 9.0 Hz, 1H, HAr), 6.76 (dd, J = 9.0, 3.1 Hz, 1H, HAr), 3.98 (d, J = 2.4 Hz, 2H, CH_2), 3.82 (s, 3H, OCH_3), 3.73 (s, 3H, OCH_3); **^{13}C NMR** (126 MHz, DMSO-d_6) δ = 173.78, 170.22, 164.91, 153.27, 145.70, 135.62, 133.70, 132.94, 132.19, 129.76, 129.23, 128.66, 127.89, 127.50, 126.81, 112.49, 110.62, 110.13, 56.62, 55.81, 34.50; **HRMS** (TOF ESI$^+$): m/z calcd for $C_{26}H_{22}N_2O_5$ [M+Na]$^+$, 465.1421, found, 465.1422.

(N-(4-(Difluoromethoxy)phenyl)-3-((2,5-dioxo-1-phenylpyrrolidin-3-ylidene)methyl)benzamide (g17)

Yellow solid; M.p. 213-214 °C; **^{1}H NMR** (500 MHz, DMSO-d_6) δ = 10.46 (s, 1H, HN), 8.22 (s, 1H, HAr_2), 8.03 (d, J = 8.0 Hz, 1H, HAr_2), 7.94 (d, J = 6.7 Hz, 1H, HAr_2), 7.85 (d, J = 9.0 Hz, 2H, HAr_1), 7.72 – 7.64 (m, 2H, HAr and C=CH), 7.54 (t, J = 7.6 Hz, 2H, HAr), 7.46 (t, J = 7.5 Hz, 1H, FCHF), 7.43 – 7.37 (m, 2H, HAr), 7.28 – 7.17 (m, 3H, HAr), 3.97 (d, J = 2.4 Hz, 2H, CH_2); **^{13}C NMR** (126 MHz, DMSO-d_6) δ = 173.76, 170.21, 165.38, 147.14, 136.68, 135.94, 134.63, 133.34, 132.94, 132.19, 129.75, 129.65, 129.36, 129.21, 128.84, 128.67, 127.49, 126.80, 122.26, 119.75, 118.92, 116.87, 114.82, 34.44; **HRMS** (TOF ESI$^+$): m/z calcd for $C_{25}H_{18}F_2N_2O_4$ [M+Na]$^+$, 471.1127, found, 471.1124.

3-((2,5-Dioxo-1-phenylpyrrolidin-3-ylidene)methyl)-N-(4-methoxy-2-methylphenyl)benzamide (g18)

Yellows solid; M.p. 238-239 °C; **^{1}H NMR** (500 MHz, DMSO-d_6) δ = 9.92 (s, 1H, HN), 8.23 (s, 1H, HAr_2), 8.04 (d, J = 6.4 Hz, 1H, HAr_2), 7.92 (d, J = 8.4 Hz, 1H, HAr_2), 7.67 – 7.64 (m, 2H), 7.57 – 7.50 (m, 2H, HAr and C=CH), 7.45 (t, J = 7.4 Hz, 1H, HAr), 7.39 (d, J = 8.3 Hz, 2H, HAr), 7.26 (d, J = 8.6 Hz, 1H, HAr), 6.89 (s, 1H, HAr), 6.81 (dd, J = 8.7, 2.8 Hz, 1H, HAr), 3.98 (s, 2H, CH_2), 3.77 (s, 3H, OCH_3), 2.25 (s, 3H, $ArCH_3$); **^{13}C NMR** (125MHz, DMSO-d_6): δ = 173.82, 170.24, 165.25, 157.80, 135.93, 135.75, 134.65, 133.52, 132.95, 132.25, 129.67, 129.42, 129.21, 128.66, 128.42, 127.51, 126.73, 115.76, 111.69, 55.54, 34.47, 18.50; **HRMS** (TOF ESI$^+$): m/z calcd for $C_{26}H_{22}N_2O_4$ [M+Na]$^+$, 449.1471, found, 449.1467.

3-((2,5-Dioxo-1-phenylpyrrolidin-3-ylidene)methyl)-N-(4-ethylphenyl)benzamide (g19)

Yellows solid; M.p. 212-213 °C; **^{1}H NMR** (500 MHz, DMSO-d_6) δ = 10.30 (s, 1H, HN), 8.22 (s, 1H, HAr_2), 8.02 (d, J = 8.0 Hz, 1H, HAr_2), 7.92 (d, J = 8.3 Hz, 1H, HAr_2), 7.74 – 7.63 (m, 2H, HAr and C=CH), 7.54 (t, J = 7.7 Hz, 2H, HAr), 7.49 – 7.37 (m, 4H, HAr), 7.22 (d, J = 8.5 Hz, 2H, HAr), 6.71 (s, 1H, HAr), 3.97 (d, J = 2.4 Hz, 2H, $COCH_2$), 2.60 (q, J = 7.6 Hz, 2H, $ArCH_2$), 1.19 (t, J = 7.6 Hz, 3H, CH_3); **^{13}C NMR** (125MHz, DMSO-d_6): δ = 173.75, 170.20, 165.18, 139.69, 137.08, 136.19, 134.58, 133.18, 132.94, 132.26, 129.69, 129.59, 129.35, 129.20, 128.65, 128.23, 127.48, 126.72, 120.94, 34.44, 28.04, 16.06; **HRMS** (TOF ESI$^+$): m/z calcd for $C_{26}H_{22}N_2O_3$ [M+Na]$^+$, 433.1522, found, 433.1518.

3-((2,5-Dioxo-1-phenylpyrrolidin-3-ylidene)methyl)-N-(3-ethylphenyl)benzamide (g20)

Yellows solid; M.p. 201-202 °C; **^{1}H NMR** (500 MHz, DMSO-d_6) δ = 10.31 (s, 1H, HN), 8.22 (s, 1H, HAr_2), 8.03 (d, J = 7.8 Hz, 1H, HAr_2), 7.92 (d, J = 7.8 Hz, 1H, HAr_2), 7.71 – 7.61 (m, 4H, HAr and C=CH), 7.53 (t, J = 7.7 Hz, 2H, HAr), 7.45 (t, J = 7.4 Hz, 1H, HAr), 7.39 (d, J = 7.5 Hz, 2H, HAr), 7.28 (t, J = 7.8 Hz, 1H, HAr), 6.98 (d, J = 7.6 Hz, 1H, HAr), 3.97 (d, J = 2.4 Hz, 2H, $COCH_2$), 2.62 (q, J = 7.6 Hz, 2H, $ArCH_2$), 1.21 (t, J = 7.6 Hz, 3H, CH_3); **^{13}C NMR** (125MHz, DMSO-d_6): δ = 173.78, 170.22, 165.30, 144.60, 139.41, 136.17, 134.58, 133.27, 132.94, 132.24, 129.71, 129.61, 129.38, 129.21, 128.94, 128.66, 127.50, 126.74, 123.75, 120.19, 118.27, 34.45, 28.70, 15.94; **HRMS** (TOF ESI$^+$): m/z calcd for $C_{26}H_{22}N_2O_3$ [M+Na]$^+$, 433.1522, found, 433.1519

3-((2,5-Dioxo-1-p-tolylpyrrolidin-3-ylidene)methyl)-N-(3-fluorophenyl)benzamide (g21)

Yellow solid; M.p. 214-215 °C; **^{1}H NMR** (500 MHz, DMSO-d_6) δ = 10.26 (s, 1H, HN), 8.23 (s, 1H, HAr_2), 8.04 (d, J = 7.8 Hz, 1H, HAr_2), 7.93 (d, J = 7.8 Hz, 1H, HAr_2), 7.68 – 7.64 (m, 3H, HAr and C=CH), 7.32 (d, J = 6.5 Hz, 4H, HAr), 7.25 (d, J = 8.1 Hz, 3H, HAr), 3.95 (s, 2H, CH_2), 2.37 (s, 3H, CH_3); **^{13}C NMR** (126 MHz, DMSO-d_6) δ = 173.84, 170.28, 165.31, 157.14, 155.18, 138.17, 135.07, 134.70, 133.78, 132.01, 130.32, 129.68, 129.51, 127.54, 127.25, 126.89, 125.92, 124.72, 116.32, 116.16, 34.41, 21.13; **HRMS** (TOF ESI$^+$): m/z calcd for C25H19FN2O3 [M+Na]$^+$, 437.1272, found, 437.1274.

N-(4-chlorophenyl)-3-((2,5-dioxo-1-(p-tolyl)pyrrolidin-3-ylidene)methyl)benzamide (g22)

Yellow solid; M.p. 232-235 °C; **^{1}H NMR** (500 MHz, DMSO-d_6) δ = 10.50 (s, 1H, HN), 8.20 (s, 1H, HAr_2), 8.00 (d, J = 8.3 Hz, 1H, HAr_2), 7.93 (d, J = 7.8 Hz, 1H, HAr_2), 7.84 (d, J = 8.9 Hz, 2H, HAr), 7.70 – 7.61 (m, 2H, HAr and C=CH), 7.44 (d, J = 8.9 Hz, 2H, HAR), 7.32 (d, J = 8.0 Hz, 2H, HAr), 7.25 (d, J = 8.3 Hz, 2H, HAr), 3.95 (d, J = 2.4 Hz, 2H, CH_2), 2.37 (s, 3H, CH_3); **^{13}C NMR** (126 MHz, DMSO-d_6) δ = 173.81, 170.26, 165.52, 138.40, 138.17, 135.88, 134.65, 133.39, 132.03, 130.31, 129.76, 129.67, 129.36, 128.96, 127.82, 127.24, 126.86, 122.28, 34.40, 21.14; **HRMS** (TOF ESI$^+$): m/z calcd for $C_{25}H_{19}ClN_2O_3$ [M+Na]$^+$, 453.0976, found, 453.0978.

3-((2,5-dioxo-1-(p-tolyl)pyrrolidin-3-ylidene)methyl)-N-(3-ethylphenyl)benzamide (g23)

Yellow solid; M.p. 236-237 °C; **^{1}H NMR** (500 MHz, DMSO-d_6) δ = 10.29 (s, 1H, HN), 8.20 (s, 1H, HAr_2), 8.01 (d, J = 7.6 Hz, 1H, HAr_2), 7.91 (d, J = 7.8 Hz, 1H, HAr_2), 7.70 – 7.61 (m, 4H, HAr and C=CH), 7.32 (d, J = 8.0 Hz, 2H, HAr), 7.30 – 7.22 (m, 3H, HAr), 6.98 (d, J = 7.5 Hz, 1H, HAr), 3.95 (d, J = 2.4 Hz, 2H, $COCH_2$), 2.62 (q, J = 7.6 Hz, 2H, $ArCH_2$), 2.37 (s, 3H, CH_3); **^{13}C NMR** (126 MHz, DMSO-d_6) δ = 173.83, 170.29, 165.30, 144.59, 139.39, 138.18, 136.16, 134.60, 133.25,

132.11, 130.31, 129.68, 129.60, 129.33, 128.93, 127.25, 126.79, 123.75, 120.18, 118.26, 34.40, 28.68, 21.14, 15.93; **HRMS** (TOF ESI$^+$): m/z calcd for $C_{27}H_{24}N_2O_3$ [M+Na]$^+$, 447.1679, found, 447.1680.

3-((2,5-dioxo-1-(p-tolyl)pyrrolidin-3-ylidene)methyl)-N-(4-methoxyphenyl)benzamide (g24)

Yellow solid; M.p. 241-243 °C; **^{1}H NMR** (500 MHz, DMSO-d_6) δ = 10.25 (s, 1H, HN), 8.19 (s, 1H, HAr_2), 8.00 (d, J = 7.7 Hz, 1H, HAr_2), 7.90 (d, J = 7.8 Hz, 1H, HAr_2), 7.69 (d, J = 8.6 Hz, 2H, HAr), 7.66 – 7.60 (m, 2H, HAr and C=CH), 7.32 (d, J = 8.0 Hz, 2H, HAr), 7.25 (d, J = 7.9 Hz, 2H, HAr), 6.93 (d, J = 8.4 Hz, 2H, HAr), 3.88 (s, 2H, CH_2), 3.67 (s, 3H, OCH_3), 2.37 (s, 3H, $ArCH_3$); **^{13}C NMR** (126 MHz, DMSO-d_6) δ = 173.85, 170.30, 164.94, 155.35, 138.18, 136.24, 134.61, 133.16, 132.38, 132.18, 130.35, 129.70, 129.61, 129.31, 127.27, 126.74, 122.46, 114.71, 56.11, 34.45, 21.18; **HRMS** (TOF ESI$^+$): m/z calcd for $C_{26}H_{22}N_2O_4$ [M+Na]$^+$, 449.1472, found, 449.1471.

3-((1-Butyl-2,5-dioxopyrrolidin-3-ylidene)methyl)-N-(3-ethylphenyl)benzamide (g25)

Yellow solid; M.p. 168-169 °C; **^{1}H NMR** (500 MHz, DMSO-d_6) δ = 10.26 (s, 1H, NH), 8.16 (s, 1H, HAr_2), 7.99 (d, J = 7.9 Hz, 1H, HAr_2), 7.86 (d, J = 8.2 Hz, 1H, HAr_2), 7.66 –7.62 (m, 3H, HAr and C=CH), 7.55 (s, 1H, HAr), 7.27 (t, J = 7.8 Hz, 1H, HAr), 6.97 (d, J = 7.7 Hz, 1H, HAr), 3.81 (d, J = 2.4 Hz, 2H, $COCH_2$), 3.51 (t, J = 7.2 Hz, 2H, NCH_2), 2.62 (q, J = 7.6 Hz, 2H, $ArCH_2$), 1.53 (p, J = 7.3 Hz, 2H, CH_2CH_2), 1.28 (h, J = 7.4 Hz, 2H, CH_2CH_2), 1.21 (t, J = 7.6 Hz, 3H, CH_3), 0.90 (t, J = 7.3 Hz, 3H, CH_3); **^{13}C NMR** (125MHz, DMSO-d_6): δ = 174.60, 170.92, 165.26, 144.56, 139.40, 136.09, 134.58, 133.14, 131.47, 129.58, 129.50, 129.22, 128.90, 126.71, 123.70, 120.14, 118.22, 38.19, 33.99, 29.74, 28.68, 19.89, 15.91, 13.88; **HRMS** (TOF ESI$^+$): m/z calcd for $C_{24}H_{26}N_2O_3$[M+Na]$^+$, 413.1835, found, 413.1842.

N-butyl-3-((2,5-dioxo-1-(p-tolyl)pyrrolidin-3-ylidene)methyl)benzamide (g26)

Yellow solid; M.p. 195-197 °C; **^{1}H NMR** (500 MHz, DMSO-d_6) δ = 8.60 – 8.52 (m, 1H, HN), 8.08 (s, 1H, HAr_2), 7.91 (d, J = 7.9 Hz, 1H, HAr_2), 7.84 (d, J = 6.3 Hz, 1H, HAr_2), 7.62 – 7.55 (m, 2H, HAr and C=CH), 7.32 (d, J = 8.0 Hz, 2H, HAr), 7.25 (d, J = 6.9 Hz, 2H, HAr), 3.91 (s, 2H, $COCH_2$), 3.30 (q, J = 6.4 Hz, 2H, NCH_2), 2.36 (s, 3H, $ArCH_3$), 1.54 (p, J = 7.0 Hz, 2H, CH_2CH_2), 1.40 – 1.33 (m, 2H, CH_2CH_2), 0.92 (t, J = 7.4 Hz, 3H, CH_3); **^{13}C NMR** (126 MHz, DMSO-d_6) δ = 173.84, 170.29, 165.88, 138.14, 135.81, 134.49, 132.96, 132.20, 130.32, 129.66, 129.48, 128.96, 127.23, 126.56, 39.37, 34.40, 31.63, 21.13, 20.07, 14.11; **HRMS** (TOF ESI$^+$): m/z calcd for $C_{23}H_{24}N_2O_3$ [M+Na]$^+$, 399.1679, found, 399.1677.

3-((1-butyl-2,5-dioxopyrrolidin-3-ylidene)methyl)-N-(4-ethoxyphenyl)benzamide (g27)

Yellow solid; M.p. 217-219 °C; **^{1}H NMR** (500 MHz, DMSO-d_6) δ = 10.25 (s, 1H, NH), 8.16 (s, 1H, HAr_2), 7.98 (d, J = 7.7 Hz, 1H, HAr_2), 7.85 (d, J = 7.8 Hz, 1H, HAr_2), 7.69 (d, J = 7.2 Hz, 2H, HAr), 7.63 (t, J = 7.8 Hz, 1H, HAr), 7.55 (s, 1H, C=CH), 6.93 (d, J = 7.2 Hz, 2H, HAr), 4.01 (q, J = 7.0 Hz, 2H, OCH_2), 3.82 (s, 2H, $COCH_2$), 3.51 (t, J = 7.2 Hz, 2H, NCH_2), 1.53 (p, J = 7.3, 6.6 Hz, 2H, CH_2CH_2), 1.33 (t, J = 7.0 Hz, 3H, CH_2), 1.28 (q, J = 7.3, 6.8 Hz, 2H, CH_2CH_2), 0.90 (t, J = 7.4 Hz, 3H, CH_3); **^{13}C NMR** (126 MHz, DMSO-d_6) δ = 174.63, 170.94, 164.90, 155.28, 136.13, 134.56, 133.06, 132.35, 131.49, 129.50, 129.17, 126.66, 122.37, 114.62, 63.45, 38.18, 33.99, 29.74, 19.89, 15.06, 13.88; **HRMS** (TOF ESI$^+$): m/z calcd for $C_{24}H_{26}N_2O_4$ $[M+Na]^+$, 429.1785, found, 429.1785.

3-((1-butyl-2,5-dioxopyrrolidin-3-ylidene)methyl)-N-(3-fluorophenyl)benzamide (g28)

Yellow solid; M.p. 195-197 °C; **^{1}H NMR** (500 MHz, DMSO-d_6) δ = 10.52 (s, 1H, HN), 8.16 (s, 1H, HAr_2), 7.98 (d, J = 7.0 Hz, 1H, HAr_2), 7.88 (d, J = 7.8 Hz, 1H, HAr_2), 7.78 (d, J = 11.7 Hz, 1H, HAr), 7.65 (t, J = 7.8 Hz, 1H, HAr), 7.61 – 7.52 (m, 2H, HAr and C=CH), 7.41 (q, J = 7.6 Hz, 1H, HAr), 6.96 (t, J = 8.5 Hz, 1H, HAr), 3.81 (d, J = 2.4 Hz, 2H, $COCH_2$), 3.51 (t, J = 7.1 Hz, 2H, NCH_2), 1.53 (p, J = 7.3 Hz, 2H, CH_2CH_2), 1.28 (h, J = 7.4 Hz, 2H, CH_2CH_2), 0.90 (t, J = 7.4 Hz, 3H, CH_3); **^{13}C NMR** (126 MHz, DMSO-d_6) δ = 174.61, 170.91, 165.68, 163.40, 161.49, 141.23, 135.74, 134.65, 133.36, 131.36, 130.68, 130.61, 129.70, 129.57, 129.24, 126.82, 116.36, 110.70, 110.53, 107.46, 107.25, 38.19, 33.98, 29.74, 19.88, 13.87; **HRMS** (TOF ESI$^+$): m/z calcd for $C_{22}H_{21}FN_2O_3$ $[M+Na]^+$, 403.1428, found, 403.1430.

N-butyl-3-((1-butyl-2,5-dioxopyrrolidin-3-ylidene)methyl)benzamide (g29)

Yellow solid; M.p. 191-193 °C; **^{1}H NMR** (500 MHz, DMSO-d_6) δ = 8.54 (t, J = 5.6 Hz, 1H, HN), 8.02 (s, 1H, HAr_2), 7.87 (d, J = 8.1 Hz, 1H, HAr_2), 7.78 (d, J = 7.8 Hz, 1H, HAr_2), 7.55 (t, J = 7.7 Hz, 1H, HAr_2), 7.48 (s, 1H, C=CH), 3.77 (d, J = 2.4 Hz, 2H, $COCH_2$), 3.49 (t, J = 7.2 Hz, 2H, NCH_2), 3.28 (q, J = 6.6 Hz, 2H, $CONCH_2$), 1.52 (dt, J = 14.1, 7.5 Hz, 4H, CH_2CH_2), 1.34 (p, J = 7.4 Hz, 2H, CH_2CH_2), 1.26 (p, J = 7.4 Hz, 2H, CH_2CH_2), 0.97 – 0.82 (m, 6H, $2CH_3$); **^{13}C NMR** (126 MHz, DMSO-d_6) δ = 174.64, 170.94, 165.86, 135.73, 134.47, 132.85, 131.54, 129.39, 128.90, 128.83, 126.49, 38.16, 33.98, 31.61, 29.74, 20.06, 19.87, 14.10, 13.87; **HRMS** (TOF ESI$^+$): m/z calcd for $C_{20}H_{26}N_2O_3$ $[M+Na]^+$,365.1836, found, 365.1836.

3-((1-benzyl-2,5-dioxopyrrolidin-3-ylidene)methyl)-N-butylbenzamide (g30)

Yellow solid; M.p. 187-189 °C; **^{1}H NMR** (500 MHz, DMSO-d_6) δ = 8.56 (t, J = 5.6 Hz, 1H, HN), 8.04 (s, 1H, HAr_2), 7.89 (d, J = 8.0 Hz, 1H, HAr_2), 7.80 (d, J = 7.8 Hz, 1H, HAr_2), 7.57 (d, J = 7.8 Hz, 1H, HAr), 7.54 (s, 1H, C=CH), 7.34 – 7.27 (m, 5H, HAr), 4.70 (s, 2H, ArH_2), 3.87 (s, 2H, $COCH_2$), 3.28 (q, J = 6.6 Hz, 2H, NCH_2), 1.52 (p, J = 7.2 Hz, 2H, CH_2CH_2), 1.34 (h, J = 7.4 Hz, 2H, CH_2CH_2), 0.91 (t, J = 7.3 Hz, 3H, CH_3); **^{13}C NMR** (126 MHz, DMSO-d_6) δ = 174.52, 170.77, 165.87, 136.63, 135.76, 134.42, 132.91, 132.09, 129.42, 129.01, 128.93, 128.88, 127.95, 127.81, 126.39, 41.93, 39.36, 34.14, 31.62, 20.07, 14.12; **HRMS** (TOF ESI$^+$): m/z calcd for $C_{23}H_{24}N_2O_3$ $[M+Na]^+$,399.1679, found, 399.1679.

3-((1-Benzyl-2,5-dioxopyrrolidin-3-ylidene)methyl)-N-(3-ethylphenyl)benzamide (g31)

Yellow solid; M.p. 178-179 °C; **^{1}H NMR** (500 MHz, DMSO-d_6) δ = 10.28 (s, 1H, HN), 8.18 (s, 1H, HAr_2), 8.00 (d, J = 7.8 Hz, 1H, HAr_2), 7.87 (d, J = 7.9 Hz, 1H, HAr_2), 7.66 – 7.60 (m, 4H, HAr and C=CH), 7.33 (q, J = 8.8, 8.4 Hz, 4H, HAr), 7.27 (t, J = 7.8 Hz, 2H, HAr), 6.97 (d, J = 7.6 Hz, 1H, HAr), 4.71 (s, 2H, ArH_2N), 3.90 (d, J = 2.3 Hz, 2H, $COCH_2$), 2.62 (q, J = 7.6 Hz, 2H, $ArCH_2$), 1.20 (t, J = 7.6 Hz, 3H, CH_3); **^{13}C NMR** (125MHz, DMSO-d_6): δ = 174.48, 170.75, 165.27, 144.58, 139.40, 136.63, 136.11, 134.54, 133.19, 132.02, 129.53, 129.32, 128.90, 127.97, 127.82, 126.60, 123.73, 120.17, 118.25, 41.96, 34.14, 28.69, 15.92; **HRMS** (TOF ESI$^+$): m/z calcd for $C_{27}H_{24}N_2O_3$ $[M+Na]^+$, 447.1679, found, 403.47.1680.

3-((1-benzyl-2,5-dioxopyrrolidin-3-ylidene)methyl)-N-(4-ethoxyphenyl)benzamide (g32)

Yellow solid; M.p. 243-245 °C; **^{1}H NMR** (500 MHz, DMSO-d_6) δ = 10.22 (s, 1H, HN), 8.16 (s, 1H, HAr_2), 7.99 (d, J = 7.5 Hz, 1H, HAr_2), 7.86 (d, J = 7.8 Hz, 1H, HAr_2), 7.68 (d, J = 8.5 Hz, 2H, HAr), 7.63 (t, J = 7.8 Hz, 1H, HAr), 7.59 (s, 1H, C=CH), 7.39 – 7.24 (m, 5H, HAr), 6.93 (d, J = 9.0 Hz, 2H, HAr), 4.71 (s, 2H, $ArCH_2N$), 4.01 (q, J = 7.2 Hz, 2H, OCH_2), 3.90 (s, 2H, $COCH_2$), 1.32 (t, J = 7.0 Hz, 3H, CH_3); **^{13}C NMR** (126 MHz, DMSO-d_6) δ = 174.50, 170.77, 164.90, 155.29, 136.62, 136.15, 133.08, 132.33, 132.03, 129.60, 129.52, 129.26, 128.89, 127.95, 127.82, 126.56, 122.39, 114.64, 63.46, 41.94, 34.14, 15.07; **HRMS** (TOF ESI$^+$): m/z calcd for $C_{27}H_{24}N_2O_4$ $[M+Na]^+$, 463.1628, found, 463.1629.

3-((1-benzyl-2,5-dioxopyrrolidin-3-ylidene)methyl)-N-(4-chlorophenyl)benzamide (g33)

Yellow solid; M.p. 184-186 °C; **^{1}H NMR** (500 MHz, DMSO-d_6) δ = 10.45 (s, 1H, HN), 8.16 (s, 1H, HAr_2), 7.99 (d, J = 8.1 Hz, 1H, HAr_2), 7.88 (d, J = 8.1 Hz, 1H, HAr_2), 7.86 (d, J = 8.6 Hz, 2H, HAr), 7.67 – 7.56 (m, 2H, HAr and C=CH), 7.43 (d, J = 8.7 Hz, 2H, HAr), 7.32 (d, J = 6.2 Hz, 5H, HAr),

4.71 (s, 2H, $ArCH_2N$), 3.90 (s, 2H, CH_3); **^{13}C NMR** (126 MHz, DMSO-d_6) δ = 174.45, 170.73, 165.49, 138.39, 136.61, 135.84, 134.58, 133.31, 131.93, 129.76, 129.57, 129.33, 128.95, 128.88, 127.97, 127.82, 126.69, 122.27, 41.96, 34.15; **HRMS** (TOF ESI$^+$): m/z calcd for $C_{25}H_{19}ClN_2O_3$ $[M+Na]^+$, 453.0976, found, 453.0977.

*4.1.2 Synthesis of 3-((2,5-dioxo-1-(p-tolyl)pyrrolidin-3-yl)methyl)-N-(4-methoxyphenyl)benz amide (***g34***)*

Compound **g24** (1 mmol) and catalyst Pd/C (0.05 mmol) were placed in a 25-mL tube equipped with a magnet stirrer bar. Methanol (10.0 mL) was added to the mixture under a nitrogen atmosphere. The reaction system was vacuum-pumped, and then purged three times with hydrogen (1atm). The reaction mixture was stirred at r.t. for 6 h, and then resultant solution was filtrated for removal of solid catalysts, evaporated to dryness, and followed by column chromatography separation. The target product was obtained with the yield 93%.

Yellow solid; M.p. 192-194 °C; **^{1}H NMR** (500 MHz, DMSO-d_6) δ = 10.22 (s, 1H, HN), 7.83 – 7.71 (m, 2H, HAr), 7.72 – 7.60 (m, 2H, HAr), 7.50 – 7.46 (m, 1H,HAr), 7.34 (d, J = 7.6 Hz, 1H, HAr), 7.11 (d, J = 1.2 Hz, 4H, HAr), 6.91 – 6.80 (m, 2H, HAr), 3.69 (s, 3H, OCH_3), 3.29 (q, J = 6.8 Hz, 1H, CH), 2.83 (dd, J = 6.5, 1.3 Hz, 2H, $ArCH_2$), 2.35 (d, J = 7.1 Hz, 2H, $COCH_2$), 2.28 (s, 3H, CH_3); **^{13}C NMR** (126 MHz, DMSO-d_6) δ = 175.82, 175.80, 165.32, 156.60, 138.82, 137.15, 134.25, 131.43, 130.65, 129.61, 128.79, 127.17, 126.40, 125.79, 123.45, 122.32, 114.30, 55.54, 47.22, 34.01, 33.85, 21.12; **HRMS** (TOF ESI$^+$): m/z calcd for $C_{26}H_{24}N_2O_4$ $[M+Na]^+$, 451.1628, found, 451.1630.

4.2 biological assay

4.2.1 Cell growth inhibition assay

Growth inhibition of human cancer cells by **XCF-37b** was assessed via MTT assay, using DMSO as a control. HCT116, HT29, NCM460, SW480, HT29, PC-3, and HepG2 cells were grown in DMEM media with 10% FBS. The human cancer cell lines were treated with compounds at various concentrations. After a 72-h incubation, MTT [3-(4,5-dimethylthiazol- 2-yl)-2,5-diphenyl tetrazolium bromide] was added to the wells (50 μL; 0.4 mg/mL) and incubated another 4 h. The medium was aspirated, and DMSO (150 μL) was added to each well. Absorbance was measured at 490 nm using 2030 Multi-label Reader (Perkin-Elmer Victor X5, USA). Compound concentrations yielding 50% growth inhibition (IC_{50}) were calculated.

4.2.2 Cell proliferation assay

HUVECs were seeded in 96-well plates and incubated for 24 h. Cells were then starved in M200 medium containing 2% FBS for 16 h. After starvation, cells were pretreated for 30 min with the indicated concentration of **XCF-37b** (0.1, 1, 10, 20, or 40 μM), followed by VEGF stimulation (25 ng/mL) for 24 h. Cell viability was then determined via MTT assay.

4.2.3 Wound-healing migration assay

HUVECs were seeded and grown into full confluence in 6-well plates. Cells were starved with 2% FBS M200 media for 12 h to inactivate cell proliferation, then wounded by pipette tips. Fresh M200 medium with 25 ng/mL VEGF containing a vehicle or 2.5 μM sunitinib and **XCF-37b** (1, 2.5 μM) were added to the scratched monolayers. Images were taken after 0, 6, 12, and 24 hours using an inverted microscope (magnification, 10×; Nikon).

4.2.4 Chick chorioallantoic membrane (CAM) assay in fertilized chicken eggs

The effect of **XCF-37b** on *ex vivo* angiogenesis was determined via CAM assay. Briefly, fertile leghorn chicken eggs (Poultry Breeding Farm, Kunming, China) were incubated in an incubator at 37.8°C with 40% humidity. A small opening was made aseptically at the top of the live eggs on day 7. Indicated concentrations of **XCF-37b**, sunitinib and 0.9% NaCl (negative control) were mixed with DMSO and tipped on the filter paper, then gently placed on the CAM. The eggs were incubated for 48 h, then fixed with methanol and photographed. Data were quantified with Image-Pro Plus 6.0 software by counting the nascent vessels.

4.2.5 Rat aortic ring assay

The aortas of Sprague-Dawley rats anesthetized with 3% pentobarbital sodium were isolated, rinsed with opti-MEM medium and cut into 1-mm ring slices. The slices were then placed into 96-well plates embedded with 50 μL Matrigel per well and incubated at 37°C for 1 h. The opti-MEM medium with 2.5% FBS and 30 ng/mL VEGF were subsequently added to each well with the indicated test compound concentrations. On day 7, images were taken through an inverse microscope.

4.2.6 Tube formation assay

Thawed Matrigel (100 μL) was added to a prechilled 96-well plate and incubated at 37°C for 1 h. Next, 2×10^4 HUVECs suspended in M200 medium with 10% FBS were added to each well,

followed by 10 ng/mL VEGF. After 20 min, the various test compound concentrations were added to each well and incubated at 37°C for 6 h. Cells were then photographed.

4.2.7 In vivo angiogenesis assay

Balb/c nude mice (6–8 weeks old) were divided into three groups and subcutaneously injected with 400 μL Matrigel alone or with VEGF (250 ng/mL) and/or **XCF-37b**. Fifteen days later, mice were sacrificed, and the Matrigel plug was removed, weighed and photographed.

4.2.8 Transwell assay

The bottom chambers of a transwell plate were filled with M200 medium containing 10% FBS, and the top chambers were seeded with 1×10^4 HUVECs and 200 μL M200 medium without FBS. The top chamber contained the vehicle and various concentrations of the test compounds. After incubation for 6 h at 37°C, cells that migrated to the bottom of the membrane were fixed with 4% paraformaldehyde and stained with 0.1% crystal violet. The migrated cells were then imaged and quantified under an inverse microscope.

4.2.9 Annex-V assay

Cells at 5×10^5 were plated into 6-well plates and treated with **XCF-37b** (1, 5, 10 and 20 μM) for 24 h. The detached and adherent cells were pooled and washed in ice-cold PBS. Following centrifugation, the supernatants were discarded, and the cells were resuspended in 1 mL fresh medium. Cells were counted, 1×10^5 cells were transferred to a fresh tube, and 100 μL annexin-V buffer plus 5 μL annexin-V-FITC were added to each sample. Samples were incubated in the dark for 20 min before further adding 400 μL annexin-V buffer and 10 μL PI (50 μg/mL), then analyzed via flow cytometry.

4.2.10 Gelatin zymography assay

Gelatinase zymography was used to analyze the effect of **XCF-37b** on the activities of MMP-2 and MMP-9 in HT29 cells. HT29 cells were treated with different concentrations of **XCF-37b** (1, 5, 10, or 20 μM) for 24 h. The culture supernatant was collected, mixed with nonreducing sample buffer, and subjected to electrophoresis on 10% SDS-PAGE with 2% gelatin. After electrophoresis, the gel was washed with 2% Triton X-100 to remove the SDS and incubated in buffer (50 mmol/L Tris pH 7.5, 150 mmol/L NaCl, 10 mmol/L $CaCl_2$ and 0.02% NaN_3) for 48h at 37°C. Gels were stained with 0.05% Coomassie brilliant blue R-250 solution (0.05% Coomassie brilliant blue R-250，30%

methanol, and 10% acetic acid). The nonstained regions in the gel corresponding to MMP-9 and MMP-2 were quantified using ImageJ software.

4.2.11 RT-qPCR

Human colon carcinoma HT29 cells were treated with **XCF-37b** (1, 5, 10, or 20 μM) for 24 h.

Total RNA was isolated from the mRMECs or HRMECs using TRIzol reagent (Invitrogen, Carlsbad, CA, USA) per the manufacturer's instructions. Quantitative reverse transcription polymerase chain reaction (RT-qPCR) was performed using an ABI ViiA7 Real-time PCR system (Thermo Scientific, Waltham, MA, USA). The Reverse Transcription System (Promega, Madison, WI, USA) was used to generate cDNA from 2 μg total RNA with random primers. Quantitative PCR was carried out using Power SYBR Green PCR master mix (Thermo Scientific) per the manufacturer's instructions. Forty amplification cycles, consisting of 5 s at 95°C and 60 s at 60°C, were run on 20-μL reactions. Taq-Man Gene Expression Assays (Thermo Scientific) were used to analyze gene expression in mRMECs following the manufacturer's instructions. TaqMan probes (Thermo Scientific) used in the RT-qPCR were Gapdh (Mm00484668_m1), HIF-1α (Hs00153153_m1), and VEGFa (Mm00437306_m1). The Gapdh expression level was used as a reference to normalize gene expression. The data were analyzed and expressed as relative gene expressions using the $2^{-\Delta\Delta CT}$ method. **Table 3** lists the PCR primer sequences used.

Table 3. Primer Sequences for RT-qPCR Analysis

HIF-1α	Forward	CATAAAGTCTGCAACATGGAAGGT
	Reverse	ATTTGATGGGTGAGGAATGGGTT
GAPDH	forward	GGAGCGAGATCCCTCCAAAAT
	Reverse	GGCTGTTGTCATACTTCTCATGG
VEGF-A	forward	CAACATCACCATGCAGATTATGC
	Reverse	CCCACAGGGATTTTCTTGTCTT

4.2.12 Western blot assay

To determine the effects of **XCF-37b** on the VEGFR-2-dependent signaling pathway, HUVECs were serum-starved overnight, then pretreated with or without **XCF-37b** (1, 2.5, 5, or 10 μM) for 2 h, followed by stimulation with 50 ng/mL $VEGF_{165}$ for 15 min. Cells were lysed with buffer containing 20 mmol/L Tris, 2.5 mmol/L EDTA, 1% Triton X-100, 1% deoxycholate, 0.1% SDS, 40 mmol/L NaF, 10 mmol/L $Na_4P_2O_7$, proteinase inhibitor cocktail and 1 mmol/L phenylmethylsulfonyl fluoride. Protein concentrations were determined via Bradford assay and equalized before loading. Approximately 20 μg of cellular proteins were separated using gradient

SDS-PAGE gels and probed with specific antibodies (Cell Signaling Technology) including phospho-VEGFR2 (p-VEGFR2; Tyr1175), VEGFR2, phospho-ERK1/2 (p-ERK1/2; Thr202/Tyr204), ERK, phospho-AKT (p-AKT; Ser473), AKT and actin. Blots were developed by incubating them with horseradish peroxidase-conjugated antibodies (GE Health Care, UK) and visualized using enhanced chemiluminescence reagent (Thermo).

4.2.13 In vitro kinase screening

Kinase screening was performed by Kebai Biotechnology Co., Ltd. (Nanjing, Jiangsu, China) and used to screen for compound **XCF-37b**. The assay protocol was as follows. In a final reaction volume of 25 μL, kinase (5–10 mU) was incubated with 25 mM Tris pH 7.5, 0.02 mM EGTA, 0.66 mg/mL myelin basic protein, 10 μM magnesium acetate and [γ^{33}p-ATP] (specific activity approx. 500 cpm/pmol concentration as required). The reaction was initiated by adding the Mg-ATP mix. After incubation for 40 min at room temperature, the reaction was stopped by adding 5 μL of a 3% phosphoric acid solution. Ten microliters of the reaction was then spotted onto P30 filter material and washed three times for 5 min in 75 mM phosphoric acid and once in methanol prior to drying and scintillation counting.

4.2.14 Tumor xenograft experiments

Nude mice were housed and maintained under specific pathogen-free conditions per institutional animal care and use committee protocol. HT29 cells were subcutaneously injected into the right flanks of nude mice. When the tumors reached approximately 100 mm^3, the mice were randomly assigned to the control or treatment group. The control group received the vehicle (0.9% NaCl) alone, and the treatment group received **XCF-37b** (20, 40 and 60 mg/kg) and sunitinib (40 mg/kg) (p.o.). The compounds were administered for 7 days, then 20 days later, the mice were sacrificed, and normal and tumor tissues were collected for molecular assessment. The body weight and tumor size of each mouse was measured every other day. Exercised tumor and normal tissues were fixed, processed, and embedded. Histology was assessed by staining with hematoxylin and eosin (H&E). The tumor sections were immunohistochemically stained with anti-CD31, anti-Ki-67, and anti-p-mTOR antibodies. A TUNEL assay was conducted following the manufacturer's instructions. Quantitation was conducted using IPP 6.0 and GraphPad software.

4.3 Molecular docking

Molecular docking of compound **XCF-37b** into the three-dimensional X-ray structure of kinase

proteins (VEGFR PDB code: 3WZE; mTOR PDB code: 4JT6) was performed using GoldDock 5.0. The three-dimensional structure of **XCF-37b** was constructed using Chemoffice 3D ultra 13.0 software, then energetically minimized using MMFF94 with 10000 iterations and a minimum RMS gradient of 0.10. The kinase crystal structures were retrieved from the RCB Protein Data Bank (http://www.rcsb.org). All bound waters and ligands were eliminated, and the polar hydrogen was added. The whole protein was defined as a receptor, and the site sphere was selected based on the kinase binding site. Compound **XCF-37b** was placed during the molecular docking procedure. Interaction types of the proteins docked with ligands were analyzed after the docking was complete.

Conflict of Interest

None of the authors of the above manuscript has declared any conflict of interest which may arise from being named as an author on the manuscript.

Acknowledgments

This work was supported by the National Natural Science Foundation of China (Nos. 21662044, 81560601, 21262043, 81760621, and U1202221); Training Program for Young and Middle-aged Academic and Technical Leaders in Yunnan Province (2015HB004); the Program for Changjiang Scholars and Innovative Research Team in University (IRT17R94); the Foundation of “Yunling Scholar” Program of Yunnan Province (C6183005); the 2017 Medical Oncology Academic leader training program from the Health and Family Planning Commission of Yunnan province (D-2017001); and thank the High Performance Computing Center at Yunnan University for use of the high performance computing platform.

Author Contributions

Yi Jin, Jihong Zhang, and Jun Lin conceived and planned the experiments. Kaixiu Luo, Yafeng Bao, Feifei Liu, and Chuanfan Xiao carried out the experiments. Ke Li, Conghai Zhang and Rong Huang carried out the spectral analysis of compounds. Yi Jin, Jihong Zhang, and Jun Lin contributed to the interpretation of the results. Yi Jin took the lead in writing the manuscript. All authors provided critical feedback and helped shape the research, analysis, and manuscript.

Reference

1. Zhao, Y. L.; Hu, X. Q.; Zuo, X. Y.; Wang, M. F. Chemopreventive effects of some popular phytochemicals on

human colon cancer: a review. *Food Funct.* **2018,** 9, 4548-4568.

2. Montminy, E. M.; Karlitz, J. J.; Landreneau, S. W. Progress of colorectal cancer screening in United States: Past achievements and future challenges. *Prev. Med.* **2019,** 120, 78-84.
3. Sarvizadeh, M.; Malekshahi, Z. V.; Razi, E.; Sharifi, H.; Moussavi, N.; Taghizadeh, M. MicroRNA: A new player in response to therapy for colorectal cancer. *J. Cell. Physiol.* **2019,** 234, 8533-8540.
4. Modest, D. P.; Pant, S.; Sartore-Bianchi, A. Treatment sequencing in metastatic colorectal cancer. *Eur. J. Cancer* **2019,** 109, 70-83.
5. Serrano, D.; Bonanni, B.; Brown, K. Therapeutic cancer prevention: achievements and ongoing challenges - a focus on breast and colorectal cancer. *Mol. Oncol.* **2019,** 13, 579-590.
6. Mirzaei, H.; Salehi, H.; Sahebkar, A.; Avan, A.; Jaafari, M. R.; Namdar, A.; Rezaei, A.; Mirzaei, H. R. Deciphering biological characteristics of tumorigenic subpopulations in human colorectal cancer reveals cellular plasticity. *J. Res. Med. Sci.* **2016,** 21.
7. Foubert, F.; Matysiak-Budnik, T.; Touchefeu, Y. Options for metastatic colorectal cancer beyond the second line of treatment. *Digest. Liver Dis.* **2014,** 46, 105-112.
8. Parizadeh, S. M.; Jafarzadeh-Esfehani, R.; Hassanian, S. M.; Parizadeh, S. M. R.; Vojdani, S.; Ghandehari, M.; Ghazaghi, A.; Khazaei, M.; Shahidsales, S.; Rezayi, M.; Asgharzadeh, F.; Ghayour-Mobarhan, M.; Ferns, G. A.; Avan, A. Targeting cancer stem cells as therapeutic approach in the treatment of colorectal cancer. *The international journal of biochemistry & cell biology* **2019,** 110, 75-83.
9. Moridikia, A.; Mirzaei, H.; Sahebkar, A.; Salimian, J. MicroRNAs: Potential candidates for diagnosis and treatment of colorectal cancer. *J. Cell. Physiol.* **2018,** 233, 901-913.
10. Peng, W.; Zhang, S.; Zhang, Z.; Xu, P.; Mao, D.; Huang, S.; Chen, B.; Zhang, C.; Zhang, S. Jianpi Jiedu decoction, a traditional Chinese medicine formula, inhibits tumorigenesis, metastasis, and angiogenesis through the mTOR/HIF-1 alpha/VEGF pathway. *J. Ethnopharmacol.* **2018,** 224, 140-148.
11. Lopez, A.; Harada, K.; Vasilakopoulou, M.; Shanbhag, N.; Ajani, J. A. Targeting Angiogenesis in Colorectal Carcinoma. *Drugs* **2019,** 79, 63-74.
12. Folkman, J. Tumor angiogenesis: therapeutic implications. *N. Engl. J. Med.* **1971,** 285, 1182-6.
13. Hurwitz, H.; Fehrenbacher, L.; Novotny, W.; Cartwright, T.; Hainsworth, J.; Heim, W.; Berlin, J.; Baron, A.; Griffing, S.; Holmgren, E.; Ferrara, N.; Fyfe, G.; Rogers, B.; Ross, R.; Kabbinavar, F. Bevacizumab plus irinotecan, fluorouracil, and leucovorin for metastatic colorectal cancer. *N. Engl. J. Med.* **2004,** 350, 2335-42.
14. Ferrara, N.; DavisSmyth, T. The biology of vascular endothelial growth factor. *Endocr. Rev.* **1997,** 18, 4-25.

15. Liu, Y. C.; Wu, R. H.; Wang, W. S. Regorafenib diminishes the expression and secretion of angiogenesis and metastasis associated proteins and inhibits cell invasion via NF-kappa B inactivation in SK-Hep1 cells. *Oncol. Lett.* **2017,** 14, 461-467.

16. Zibara, K.; Awada, Z.; Dib, L.; El-Saghir, J.; Al-Ghadban, S.; Ibrik, A.; El-Zein, N.; El-Sabban, M. Anti-angiogenesis therapy and gap junction inhibition reduce MDA-MB-231 breast cancer cell invasion and metastasis in vitro and in vivo. *Sci Rep-Uk* **2015,** 5.

17. Mahecha, A. M.; Wang, H. B. The influence of vascular endothelial growth factor-A and matrix metalloproteinase-2 and-9 in angiogenesis, metastasis, and prognosis of endometrial cancer. *Oncotargets Ther.* **2017,** 10, 4617-4624.

18. Dey, N.; De, P.; Leyland-Jones, B. PI3K-AKT-mTOR inhibitors in breast cancers: From tumor cell signaling to clinical trials. *Pharmacol. Therapeut.* **2017,** 175, 91-106.

19. Sharma, S.; Guru, S. K.; Manda, S.; Kumar, A.; Mintoo, M. J.; Prasad, V. D.; Sharma, P. R.; Mondhe, D. M.; Bharate, S. B.; Bhushan, S. A marine sponge alkaloid derivative 4-chloro fascaplysin inhibits tumor growth and VEGF mediated angiogenesis by disrupting PI3K/Akt/mTOR signaling cascade. *Chem-Biol. Interact.* **2017,** 275, 47-60.

20. Ma, J. C.; Sun, X. W.; Su, H.; Chen, Q.; Guo, T. K.; Li, Y.; Chen, X. C.; Guo, J.; Gong, Z. Q.; Zhao, X. D.; Qi, J. B. Fibroblast-derived CXCL12/SDF-1 alpha promotes CXCL6 secretion and co-operatively enhances metastatic potential through the PI3K/Akt/mTOR pathway in colon cancer. *World J. Gastroentero.* **2017,** 23, 5167-5178.

21. Han, C. Z.; Xing, G. Z.; Zhang, M. Y.; Zhong, M.; Han, Z.; He, C. Y.; Liu, X. P. Wogonoside inhibits cell growth and induces mitochondrial-mediated autophagy-related apoptosis in human colon cancer cells through the PI3K/AKT/mTOR/p70S6K signaling pathway. *Oncol. Lett.* **2018,** 15, 4463-4470.

22. Lien, G. S.; Lin, C. H.; Yang, Y. L.; Wu, M. S.; Chen, B. C. Ghrelin induces colon cancer cell proliferation through the GHS-R, Ras, PI3K, Akt, and mTOR signaling pathways. *Eur. J. Pharmacol.* **2016,** 776, 124-131.

23. Thirusangu, P.; Vigneshwaran, V.; Ranganatha, V. L.; Avin, B. R. V.; Khanum, S. A.; Mahmood, R.; Jayashree, K.; Prabhakar, B. T. A tumoural angiogenic gateway blocker, Benzophenone-1B represses the HIF-1 alpha nuclear translocation and its target gene activation against neoplastic progression. *Biochem. Pharmacol.* **2017,** 125, 26-40.

24. Semenza, G. L. Defining the role of hypoxia-inducible factor 1 in cancer biology and therapeutics. *Oncogene* **2010,** 29, 625-634.

25. Noberasco, C.; Spitaleri, G.; Mancuso, P.; Milani, A.; Rocca, A.; Bertolini, F.; Curigliano, G.; de Pas, T.; Boselli, S.; de Braud, F. Combination of non-cytotoxic agents with anti-angiogenic activity for metronomic therapy of solid

tumors: Antitumor activity and biological effects. *Ann. Oncol.* **2007,** 18, 87-87.

26. Corson, T. W.; Briggs, C.; Sulaiman, R. S.; Mahoui, A.; Sishtla, K.; Shadmand, M. A non-cytotoxic compound blocks angiogenesis and decreases tumor burden in the TAg-RB retinoblastoma mouse. *Invest. Ophth. Vis. Sci.* **2017,** 58.
27. Zhang, Q.; Teng, Y.; Yuan, Y.; Ruan, T. T.; Wang, Q.; Gao, X.; Zhou, Y.; Han, K. L.; Yu, P.; Lu, K. Synthesis and cytotoxic studies of novel 5-phenylisatin derivatives and their anti-migration and anti-angiogenic evaluation. *Eur. J. Med. Chem.* **2018,** 156, 800-814.
28. Wang, J. Q.; Chen, D. M.; Li, B.; He, J.; Duan, D. L.; Shao, D. D.; Nie, M. F. Fe-MIL-101 exhibits selective cytotoxicity and inhibition of angiogenesis in ovarian cancer cells via downregulation of MMP. *Sci Rep-Uk* **2016,** 6.
29. Shrestha, R.; Shen, Y. F.; Pollack, K. A.; Taylor, J. S. A.; Wooley, K. L. Dual Peptide Nucleic Acid- and Peptide-Functionalized Shell Cross-Linked Nanoparticles Designed to Target mRNA toward the Diagnosis and Treatment of Acute Lung Injury. *Bioconjugate. Chem.* **2012,** 23, 574-585.
30. Hammami, A.; Raouafi, N.; Mirsky, V. M. Electrically controlled Michael addition: Addressing of covalent immobilization of biological receptors. *Biosens. Bioelectron.* **2018,** 121, 72-79.
31. Polepally, P. R.; Huben, K.; Vardy, E.; Setola, V.; Mosier, P. D.; Roth, B. L.; Zjawiony, J. K. Michael acceptor approach to the design of new salvinorin A-based high affinity ligands for the kappa-opioid receptor. *Eur. J. Med. Chem.* **2014,** 85, 818-829.
32. Freiberg, C.; Fischer, H. P.; Brunner, N. A. Discovering the mechanism of action of novel antibacterial agents through transcriptional profiling of conditional mutants. *Antimicrob. Agents. Ch.* **2005,** 49, 749-759.
33. Sashidhara, K. V.; Singh, S. P.; Kant, R.; Maulik, P. R.; Sarkar, J.; Kanojiya, S.; Ravi Kumar, K. Cytotoxic cycloartane triterpene and rare isomeric bisclerodane diterpenes from the leaves of Polyalthia longifolia var. pendula. *Bioorg. Med. Chem. Lett.* **2010,** 20, 5767-71.
34. Nowak-Sliwinska, P.; Storto, M.; Cataudella, T.; Ballini, J.-P.; Gatz, R.; Giorgio, M.; van den Bergh, H.; Plyte, S.; Wagnières, G. Angiogenesis inhibition by the maleimide-based small molecule GNX-686. *Microvasc. Res.* **2012,** 83, 105-110.
35. Webb, S. Back on target. *Nat. Biotechnol.* **2013,** 31, 191-193.
36. Fontaine, S. D.; Reid, R.; Robinson, L.; Ashley, G. W.; Santi, D. V. Long-Term Stabilization of Maleimide-Thiol Conjugates. *Bioconjugate. Chem.* **2015,** 26, 145-152.
37. Lyon, R. P.; Setter, J. R.; Bovee, T. D.; Doronina, S. O.; Hunter, J. H.; Anderson, M. E.; Balasubramanian, C. L.;

Duniho, S. M.; Leiske, C. I.; Li, F.; Senter, P. D. Self-hydrolyzing maleimides improve the stability and pharmacological properties of antibody-drug conjugates. *Nat. Biotechnol.* **2014,** 32, 1059-1062.

38. Shen, B. Q.; Xu, K. Y.; Liu, L. N.; Raab, H.; Bhakta, S.; Kenrick, M.; Parsons-Reponte, K. L.; Tien, J.; Yu, S. F.; Mai, E.; Li, D. W.; Tibbitts, J.; Baudys, J.; Saadi, O. M.; Scales, S. J.; McDonald, P. J.; Hass, P. E.; Eigenbrot, C.; Nguyen, T.; Solis, W. A.; Fuji, R. N.; Flagella, K. M.; Patel, D.; Spencer, S. D.; Khawlil, L. A.; Ebens, A.; Wong, W. L.; Vandlen, R.; Kaur, S.; Sliwkowski, M. X.; Scheller, R. H.; Polakis, P.; Junutula, J. R. Conjugation site modulates the in vivo stability and therapeutic activity of antibody-drug conjugates. *Nat. Biotechnol.* **2012,** 30, 184-189.

39. Baldwin, A. D.; Kiick, K. L. Tunable Degradation of Maleimide-Thiol Adducts in Reducing Environments. *Bioconjugate. Chem.* **2011,** 22, 1946-1953.

40. Kalia, D.; Malekar, P. V.; Parthasarathy, M. Exocyclic Olefinic Maleimides: Synthesis and Application for Stable and Thiol-Selective Bioconjugation. *Angew. Chem., Int. Ed.* **2016,** 55, 1432-1435.

41. Kim, H.; Cho, S. J.; Yoo, M.; Kang, S. K.; Kim, K. R.; Lee, H. H.; Song, J. S.; Rhee, S. D.; Jung, W. H.; Ahn, J. H.; Jung, J.-K.; Jung, K.-Y. Synthesis and biological evaluation of thiazole derivatives as GPR119 agonists. *Bioorg. Med. Chem. Lett.* **2017,** 27, 5213-5220.

42. Maga, G.; Falchi, F.; Radi, M.; Botta, L.; Casaluce, G.; Bernardini, M.; Irannejad, H.; Manetti, F.; Garbelli, A.; Samuele, A.; Zanoli, S.; Este, J. A.; Gonzalez, E.; Zucca, E.; Paolucci, S.; Baldanti, F.; De Rijck, J.; Debyser, Z.; Botta, M. Toward the Discovery of Novel Anti-HIV Drugs. Second-Generation Inhibitors of the Cellular ATPase DDX3 with Improved Anti-HIV Activity: Synthesis, Structure-Activity Relationship Analysis, Cytotoxicity Studies, and Target Validation. *ChemMedChem* **2011,** 6, 1371-1389.

43. Luo, Y.; Ma, L.; Zheng, H.; Chen, L.; Li, R.; He, C.; Yang, S.; Ye, X.; Chen, Z.; Li, Z.; Gao, Y.; Han, J.; He, G.; Yang, L.; Wei, Y. Discovery of (Z)-5-(4-Methoxybenzylidene)thiazolidine-2,4-dione, a Readily Available and Orally Active Glitazone for the Treatment of Concanavalin A-Induced Acute Liver Injury of BALB/c Mice. *J. Med. Chem.* **2010,** 53, 273-281.

44. Zhang, J. Q.; Liu, T. Y.; Chen, M.; Liu, F. F.; Liu, X. Y.; Zhang, J. H.; Lin, J.; Jin, Y. Synthesis and Biological Evaluation of Indole-2-carbohydrazide Derivatives as Anticancer Agents with Anti-angiogenic and Antiproliferative Activities. *Chemmedchem* **2018,** 13, 1181-1192.

45. Xi, L.; Zhang, J. Q.; Liu, Z. C.; Zhang, J. H.; Yan, J. F.; Jin, Y.; Lin, J. Novel 5-anilinoquinazoline-8-nitro derivatives as inhibitors of VEGFR-2 tyrosine kinase: synthesis, biological evaluation and molecular docking. *Organic & Biomolecular Chemistry* **2013,** 11, 4367-4378.

46. Zhao, S. Y.; Li, K.; Jin, Y.; Lin, J. Synthesis and biological evaluation of novel 1-(aryl-aldehyde-oxime) uracil derivatives as a new class of thymidine phosphorylase inhibitors. *Eur. J. Med. Chem.* **2018,** 144, 41-51.

47. Wilhelm, S.; Carter, C.; Lynch, M.; Lowinger, T.; Dumas, J.; Smith, R. A.; Schwartz, B.; Simantov, R.; Kelley, S. Discovery and development of sorafenib: a multikinase inhibitor for treating cancer. *Nature Reviews Drug Discovery* **2006,** 5, 835-844.

48. Strumberg, D.; Scheulen, M. E.; Schultheis, B.; Richly, H.; Frost, A.; Buechert, M.; Christensen, O.; Jeffers, M.; Heinig, R.; Boix, O.; Mross, K. Regorafenib (BAY 73-4506) in advanced colorectal cancer: a phase I study. *British Journal of Cancer* **2012,** 106, 1722-1727.

49. Ratain, M. J.; Eisen, T.; Stadler, W. M.; Flaherty, K. T.; Kaye, S. B.; Rosner, G. L.; Gore, M.; Desai, A. A.; Patnaik, A.; Xiong, H. Q.; Rowinsky, L.; Abbruzzese, J. L.; Xia, C. H.; Simantov, R.; Schwartz, B.; O'Dwyer, P. J. Phase II placebo-controlled randomized discontinuation trial of sorafnib in patients with metastatic renal cell carcinoma. *J. Clin. Oncol.* **2006,** 24, 2505-2512.

50. Wang, J. M.; Liu, H. J.; Fan, Y. T.; Yang, Y. Y.; Jiang, Z. Y.; Tan, C. H. Bicyclic Guanidine-Catalyzed Direct Asymmetric Allylic Addition of N-Aryl Alkylidene-Succinimides. *Chem-Eur. J.* **2010,** 16, 12534-12537.

51. Geng, Z.; Cao, J.; Ma, X.; Li, C.; Wang, Z. Effects of polynitrogen compounds on the activity of recombinant human Hypoxia inducible factor-1 alpha prolyl hydroxylase 3 in Escherichia coli. *Faseb J.* **2011,** 25.

52. Cao, Y. H. Positive and Negative Modulation of Angiogenesis by VEGFR1 Ligands. *Sci. Signal.* **2009,** 2(59), ref1.

53. Semenza, G. L. HIF-1 and tumor progression: pathophysiology and therapeutics. *Trends Mol. Med.* **2002,** 8, S62-S67.

54. Costa, D. B. Identification of somatic genomic alterations in circulating tumors cells: another step forward in non-small-cell lung cancer? *Journal of clinical oncology : official journal of the American Society of Clinical Oncology* **2013,** 31, 2236-9.

55. Goel, H. L.; Mercurio, A. M. VEGF targets the tumour cell. *Nat. Rev. Cancer* **2013,** 13, 871-882.

56. Hanahan, D.; Folkman, J. Patterns and emerging mechanisms of the angiogenic switch during tumorigenesis. *Cell* **1996,** 86, 353-64.

57. Folkman, J. Role of angiogenesis in tumor growth and metastasis. *Seminars in oncology* **2002,** 29, 15-8.

58. Nanjing Kebai Biotechnology Co., Ltd. Web Site. Available from: www.cobioer.com.

Highlights

- The newly synthesized benzylidene-succinimide derivatives showed obvious anti-angiogenic activities with non-cytotoxicity against colorectal cancer cells and human normal cell.
- Among them, compound **XCF-37b** exerted the most excellent anti-angiogenesis *ex vivo* and *in vivo*, and also non-cytotoxicity on varied other cancer cells.
- Mechanism study confirmed that **XCF-37b** regulated angiogenic inhibition through a variety of regulatory pathways, including to inhibit AKT/mTOR and VEGFR2 signaling pathway, while no significant interference on the growth of colorectal cancer cells.